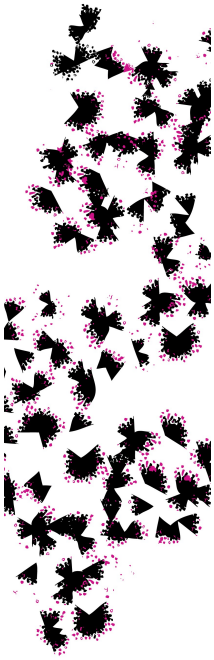

Respiratory Motion Estimation of the Liver with Abdominal Motion as a Surrogate: A Supervised Learning Approach

S. (Shamel) Fahmi

MSc Report

Committee:
Prof.dr.ir. S. Stramigioli
Dr.ir. M. Abayazid
Dr. F.J. Siepel
Dr.ir. L.J. Spreeuwers

August 2017

039RAM2017
Robotics and Mechatronics
EE-Math-CS
University of Twente
P.O. Box 217
7500 AE Enschede
The Netherlands

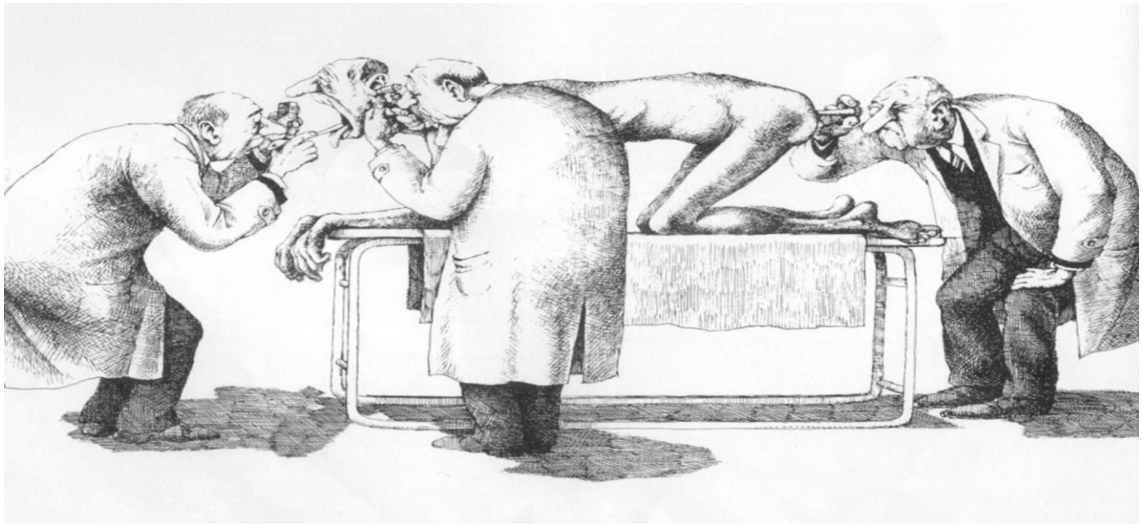

Prior Medical Imaging
Courtesy of Humour noir et hommes en blanc, de Serre, Catronné

Preface

This thesis summarizes the work and experience gained here at the University of Twente (UT) during my Masters degree in Systems and Control. A lot of people supported me during the two years in UT. Thus, I would like to explicitly recognize the following people for their support.

Firstly, I would like to express my profound gratitude to God and my family (Shamel Sr., Amal, Menna and Mohamed) for their continuous support and encouragement. To my Godfather Essam, thank you for always being there when I needed you. You were and will always be my role model. To my brothers Adel and Samer without whom this work would have been completed way earlier, thank you for reminding me how crazy I am and for being my sanity.

I would like to express my sincere gratitude to my daily supervisor Momen Abayazid for his patience, motivation, enthusiasm, and knowledge. I really enjoyed having you as a big brother and supervisor. I would like to thank Stefano Stramigioli for suggesting this topic and giving me the chance to conduct my thesis in the Robotics and Mechatronics Lab. Additionally, I would like to thank Francoise and Luuk for being a part of my graduation committee. Moreover, I would like to thank Raffaella Carloni for giving me the chance to work under her supervision during the first year of my degree.

My fervent gratitude goes to Thomas Hulin for offering me the opportunity to conduct my internship at the German Aerospace Center (DLR). As I always told Thomas, I found myself the most in DLR. I was always full with motivation and enthusiasm every single day during my internship. I am really grateful for your utmost advice. I still believe that we will meet again.

I would like to thank Jolanda for her love and care throughout my thesis. I would also like to thank Cindy, Jordy and Frank from the technical medicine department for their help during the experiments.

To Ena, thank you for your love and for handling my insanity. Most importantly thank you for being you. To Carlos, Fay, Eva, Vassilina and Pavel, thank you for being my family in Enschede. Thank you for making me feel home.

To Patricia, thank you for your support and help throughout my thesis. To Kareem, Khaled, Andrea, Eamon, Jeroen, Trisch, Saskia and Emiddio, thank you so much for your love. I still believe that the lab would have been a lot calmer without you.

To May, thank you for the nights spent on making my presentation luster. To Genarro, thank you for always reminding me that I "stress too much and work too much and shouldn't do that". Finally, to the Netherlands, thank you for having the coolest people ever and making me feel that I never left home (except that home does not have that weather and rain).

Shamel Fahmi
Enschede, August 2017

"If other people are putting in 40 hour work weeks and you're putting in 100 hour work weeks, then if you are doing the same thing you know that you will achieve in 4 months what it takes them a year to achieve" - Elon Musk

Summary

Currently, imaging techniques are advancing widely in the medical field especially during image-guided interventions and diagnosis. Among the available medical imaging techniques, magnetic resonance imaging (MRI) offers the highest soft tissue contrast, which helps detecting small lesions (such as tumors) at an early stage. However, MRI does not offer high update rate acquisitions and thus the exact motion of the lesions remains uncertain. Moreover, respiratory induced motion introduces significant challenges during medical image acquisition and image-guided interventions. Respiratory induced internal liver motion causes uncertainties in localizing hepatic lesions which could lead to motion artifacts and misdiagnoses during image acquisition or inaccurate targeting and significant tissue loss in case of image guided interventions. A common approach is Respiratory Motion Estimation (RME) in which the internal liver motion is estimated by measuring external signals called surrogates that do not directly measure the internal liver motion. The aim of this thesis is to determine the feasibility of estimating the internal motion of the liver due to respiration acquired using MRI by tracking small sized markers using a digital camera. The two acquired data will be processed offline and a fitting algorithm will be developed to design motion models such that based solely on tracking the external markers at a high update rate, the liver motion is estimated. In the same context, three healthy subjects volunteered for human subject experiments. Each volunteer was subjected to two sessions such that MRI acquired liver images were recorded alongside with camera tracked external markers. The acquired liver and abdomen motion were utilized to train three motion models (multiv-ariate, Ridge and Lasso regression models) to estimate the superior-inferior (SI) motion of the liver. The conducted human subject experiments demonstrated that the breathing patterns differ between sessions and subjects and thus, patient specific motion models were designed. The liver SI motion estimated by the motion models were compared to the true values acquired from MRI. Over the six acquired sessions, the mean absolute error (MAE) predicted by the motion models ranged between 0.8 mm and 1.9 mm.

During the period of this thesis, a medical proposal was submitted to the local medical ethical committee at the University of Twente to approve conducting the human subject experiments. The medical proposal consisted of two main documents. Firstly, a detailed measurement protocol was documented to explain the step by step procedures of the conduced human subjects experiments (Appendix [A]). Secondly, a detailed description of the study was given to the volunteers prior signing their consent (Appendix [B]). Furthermore, before conducting the human subject experiments, various preliminary experiments (Appendix C) were conducted to formulate and develop the measurement protocol.

Contents

1 Introduction

This project aims to design, develop and validate an approach to estimate the respiratory induced motion (RIM) of the liver by utilizing abdominal motion as a surrogate signal.

1.1 Context

Accounting for 9% of worldwide, the liver is considered the second main cause of cancer deaths (WHO (2017)). However, if diagnosed and treated at early stages, 30-50% of cancer cases could be prevented (WHO (2017)). Such prevention is a challenging task that requires improving awareness, diagnosis and treatment equipment. There are multiple methods to detect liver lesions depending on the stage of the cancer. Such diagnosis range from physical examination, lab tests, imaging tests and biopsy (Oberfield et al. (1989)). In the same context, liver cancer could be treated depending on the diagnosis and the stage of the cancer. Such treatment options include invasive surgeries, tumor ablation using percutaneous needle insertion, radiation therapy and chemotherapy (WHO (2017)).

The significance of utilizing imaging modalities during treatment (image-guided interventions) and diagnosis (image acquisition) are indeed crucial. For instance, Medical imaging modalities (such as computed tomography (CT), ultrasound (US), magnetic resonance imaging (MRI), fluroscopy, etc.) are extensively utilized during such acquisitions and interventions. In particular, MRI is more superior than other imaging modalities for soft tissues (such as the liver), (Stemkens et al. (2015); Preiswerk et al. (2016)). To emphasize, high quality and update rate medical images can improve the overall diagnosis and treatment of cancer patients significantly. However, such requirements are often contradicting. For instance, MRI offers high quality images for the liver at a low update rate compared to US that offers the opposite.

1.2 Problem Statement

RIM causes great challenges during image acquisition and image guided interventions. Since respiration involves the simultaneous motion of the diaphragm and the ribcage, the organs in the abdominal and thorax regions (such as lungs, liver, diaphragm, etc.) are mostly affected (Keall et al. (2006); Ehrhardt et al. (2013)). For instance, since the liver is directly attached to the diaphragm, its induced motion could range between 8-25 mm in a single direction (Langen and Jones (2001); Shimizu et al. (1999)). As a result, uncompensated RIM alongside imaging modalities that do not offer a high update rate introduces motion artifacts that significantly influence the quality of the acquired images. Motion artifacts causes uncertainty in localizing the exact tumor motion (McClelland et al. (2013)). Such issue could lead to misdiagnoses during image acquisition and tissue loss during biopsy. Furthermore, the uncertain tumor location causes further radiation exposure to healthy cells during radio therapy (Keall et al. (2006)) and further damage to healthy tissues due to inaccurate targeting in case of needle insertion and tumor ablation,

Breath holding is one common solution to RIM such that the patient is required to hold his/her breath for approximately 20 seconds while the procedure is performed during the breath hold period (Lal et al. (2012)). Moreover, respiratory gating is also a common solution to RIM in radio therapy such that the motion of the lesions are constantly scanned during normal breathing (Keall et al. (2006)). However, the radiation is delivered during a certain window of the breathing cycle. The main disadvantage of breath holding and respiratory gating is that both techniques increase the intervention time dramatically. Moreover, during breath holding, patients might feel uncomfortable to hold their breath for that long due to illness or sedation (Zhou et al. (2013)).

Additionally, Respiratory Motion Estimation (RME) is another approach that estimates the actual motion of interest by measuring external signals so called surrogate signals (Ehrhardt et al. (2013)). Surrogate signals could be any internal or external signals obtained at a tolerable temporal resolution and with a strong correlation with the internal motion of interest. The main objective of RME is given a set of surrogate and motion data, a motion model is designed that describes the relation between the surrogate and motion data. The motion model is developed by utilizing a fitting method that is typically a supervised learning algorithm which fits the surrogate to the motion data.

1.3 Goals

This context will be focusing on respiratory motion estimation of the liver such that the motion data are MRI acquired liver scans. Accordingly, the objectives of this paper are summarized as follows:

- Analyzing the types of surrogate signals and determining appropriate surrogate data that fit(s) the challenging MR environment.
- Developing motion model(s) by determining appropriate supervised learning algorithm(s) that have a strong relationship between the surrogate and motion data.
- Validating the designed motion model(s) and the suggested RME approach by conducting human subject experiments.

1.4 Outline

This thesis is outlined as follows:

- The developed RME approach and the conducted human subject experiments were summarized in paper format. Abdominal motion tracking was chosen as the optimal surrogate signal choice and was justified in the paper. Moreover, three supervised learning algorithms were chosen accordingly. Additionally, human subject experiments were conducted at an open bore MRI system at the University of Twente.
- A measurement protocol explaining the step by step procedures of the conduced human subjects experiments was submitted to the local medical ethical committee and is presented in Appendix [A].
- A brief description of the study given to the volunteers prior signing their consent was documented and presented in Appendix [B].
- Before conducting the human subject experiments, various preliminary experiments were conducted to formulate and develop the measurement protocol. The preliminary experiments are presented in Appendix [C]
- The recruitment procedures of the volunteers are presented in Appendix [D]

2 Paper: Respiratory Motion Estimation of the Liver with Abdominal Motion as a Surrogate: A Supervised Learning Algorithm

Abstract – Respiratory induced motion introduces significant challenges during image acquisition and image guided interventions. Respiratory induced internal motion causes uncertainties in localizing hepatic lesions which could lead to motion artifacts and misdiagnoses during image acquisition or inaccurate targeting and significant tissue loss in case of image guided interventions. A common approach is Respiratory Motion Estimation (RME) in which the internal liver motion is estimated by measuring external signals called surrogates. In this paper, external markers placed on the human's abdomen were measured and subsequently correlated to the internal liver motion obtained during MRI acquisition. Accordingly, appropriate correspondence models were designed to correlate the internal liver motion with the external markers motion. Three subjects volunteered for two sessions each such that MRI acquired liver images were recorded alongside with camera tracked external markers. The acquired liver and abdominal motion were utilized to train three correspondence models (multivariate, Ridge and Lasso regression models) to estimate the superior-inferior (SI) motion of the liver. The conducted human subject experiments demonstrated that the breathing patterns differ between sessions and subjects and thus, patient specific correspondence models were designed. The liver SI motion estimated by the correspondence models were compared to the true values acquired from MRI. Over the six acquired sessions, the mean absolute error (MAE) predicted by the correspondence models ranged between 0.8 mm and 1.9 mm. The results also concluded that using multiple markers can improve the estimation accuracy as well as using multiple surrogates. The authors also suggested that using high resolution (temporal and spacial) MRI images can significantly improve the overall performance of the RME framework.

Respiratory Motion Estimation of the Liver with Abdominal Motion as a Surrogate: A Supervised Learning Approach

Shamel Fahmi[1] and Momen Abayazid[1]

***Abstract*— Respiratory induced motion introduces significant challenges during image acquisition and image guided interventions. Respiratory induced internal motion causes uncertainties in localizing hepatic lesions which could lead to motion artifacts and misdiagnoses during image acquisition or inaccurate targeting and significant tissue loss in case of image guided interventions. A common approach is Respiratory Motion Estimation (RME) in which the internal liver motion is estimated by measuring external signals called surrogates. In this paper, external markers placed on the human's abdomen were measured and subsequently correlated to the internal liver motion obtained during MRI acquisition. Accordingly, appropriate motion models were designed to correlate the internal liver motion with the external markers motion. Three subjects volunteered for two sessions each such that MRI acquired liver images were recorded alongside with camera tracked external markers. The acquired liver and abdominal motion were utilized to train three motion models (multivariate, Ridge and Lasso regression models) to estimate the superior-inferior (SI) motion of the liver. The conducted human subject experiments demonstrated that the breathing patterns differ between sessions and subjects and thus, patient specific motion models were designed. The liver SI motion estimated by the motion models were compared to the true values acquired from MRI. Over the six acquired sessions, the mean absolute error (MAE) predicted by the motion models ranged between 0.8 mm and 1.9 mm. The results also concluded that using multiple markers can improve the estimation accuracy as well as using multiple surrogates. The authors also suggested that using high resolution (temporal and spacial) MRI images can significantly improve the overall performance of the RME framework.**

***Index Terms*— Respiratory Motion Estimation (RME), Magnetic Resonance Imaging (MRI), Respiratory Induced Motion (RIM), Statistical Learning, Surrogate Signals, Optical Tracking.**

I. Introduction

A. Liver Cancer

The liver is the largest organ in the human body located in the upper-right abdomen, attached to the diaphragm and guarded by the rib cage [1]. Liver cancer is the second main cause of cancer deaths worldwide accounting for approximately 9%. In the Netherlands, liver cancer accounts for 2.4% of all cancer cases [2]. Moreover, 70% of cancer deaths occur in developing countries due to the lack of diagnosis, care and prevention equipment. As stated by the World Health Organization (WHO), 30-50% of cancer cases could be prevented if diagnosed and treated early [3].

[1]S. Fahmi and M. Abayazid are with the Robotics and Mechatronics Lab, Faculty of Electrical Engineering, Mathematics and Computer Science, University of Twente, 7522 NH Enschede, The Netherlands. a.m.s.b.m.fahmi@student.utwente.nl, m.abayazid@utwente.nl.

Liver cancer diagnosis varies from physical examination, lab tests, imaging tests and biopsy [4]. Moreover, there are several treatment options for liver cancer depending on the diagnosis and the stage of the cancer. These options could be invasive surgeries, tumor ablation using percutaneous needle insertion, radiation therapy, chemotherapy, etc [3]. Percutaneous image-guided interventions are widely performed during cancer treatment. These interventions are utilized during needle insertion/biopsy, fluid collection drainage and tumor ablation and are guided using medical imaging modalities [5].

Medical imaging modalities (such as computed tomography (CT), ultrasound (US), magnetic resonance imaging (MRI), fluroscopy, etc.) are widely used during image acquisition and image guided interventions. These modalities are used depending on the type, structure and number of lesions and/or the tissue of the organ. For soft tissues (such as the liver), MRI is more preferable than other imaging modalities [6], [7]. It is important to emphasize the significance of imaging modalities during treatment (image-guided interventions) and diagnosis (image acquisition). In fact, high quality and real-time medical images can significantly improve the overall diagnosis and treatment of cancer patients. However, both requirements are usually contradicting. For instance, MRI offers high image quality at a low update rate compared to ultrasound who offers the opposite [7].

B. Respiratory Induced Motion (RIM)

Organ motion during procedures causes a huge challenge and dramatically reduces the efficiency of such procedures [8]. One of the main causes of internal organ motion is due to respiration. Respiratory motion is characterized mainly by the diaphragm and the ribcage motion due to the expansion and contraction of the lungs during inhalation and exhalation (as shown in Fig. 1). Respiratory induced motion (RIM) mainly affects the organs in the abdominal and thorax regions (such as lungs, liver, diaphragm, etc.) [9], [10]. In fact, respiratory induced liver motion could range from 8-25 mm in a single direction and is more dominant in the superior-inferior (SI) direction than the anterior-posterior (AP) and lateral directions [8], [11].

In the same context, the average human breathing frequency is 12-15 breaths per minute during normal breathing (at rest) [12]. Thus, if RIM is not compensated and the imaging modalities do not offer such an update rate, the quality of the images will be significantly influenced by motion artifacts [9]. As a result, during image acquisition,

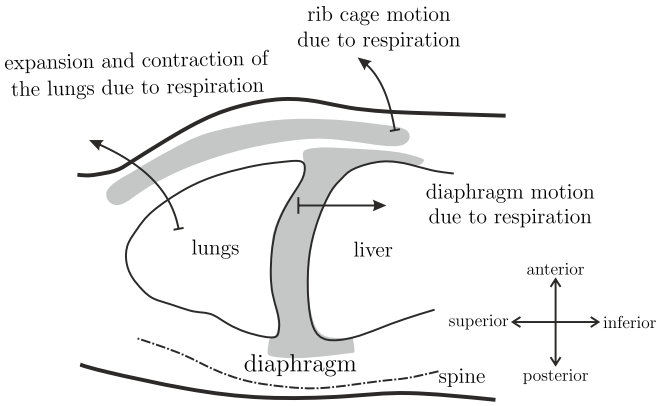

Fig. 1. Schematic sagittal slice showing respiratory induced motion (RIM) due to breathing. During respiration the lungs expand and contract due to the motion of the diaphragm and the rib cage.

motion artifacts significantly reduce the quality of the acquired images which results in an uncertainty in locating the exact tumor motion [13]. The same problem occurs during treatment in radiotherapy, the uncertain tumor location causes further radiation exposure to healthy cells which might be hazardous for the patient [9]. Furthermore, during image-guided interventions and biopsy, the exact knowledge of the lesions' locations are crucial to ensure accurate targeting. Inaccurate targeting causes further damage to healthy tissues in case of needle insertion and tumor ablation, and misdiagnoses in case of biopsy.

A common solution to RIM is breath holding. Breath holding is a technique that requires the patient to hold his/her breath for approximately 20 seconds such that treatments occur only during that period of breath hold [14]. The main disadvantage of breath holding is that it increases the intervention time dramatically. Moreover, patients might feel uncomfortable to hold his/her breath for that long due to illness or sedation [15]. Respiratory gating is also a common solution during radiotherapy such that the RIM of the lesions are constantly scanned during normal breathing [9]. Nevertheless, the radiation is delivered during a specific window of the breathing cycle henceforth the approach still suffers from the increase in acquisition and intervention time.

C. Respiratory Motion Estimation (RME)

Respiratory Motion Estimation (RME) is another approach that estimates the actual internal motion of interest by measuring external signals so called surrogate signals [10]. Surrogate signals are signals that do not measure the actual internal motion of interest but have a strong correlation with it and could be easily measured. RME is genuinely utilized in applications when it is not possible or feasible to directly acquire the actual internal motion of interest with a tolerable temporal resolution/update rate [13]. RME depends on deriving a motion model that describes the relation between the internal motion of interest with the surrogate signals.

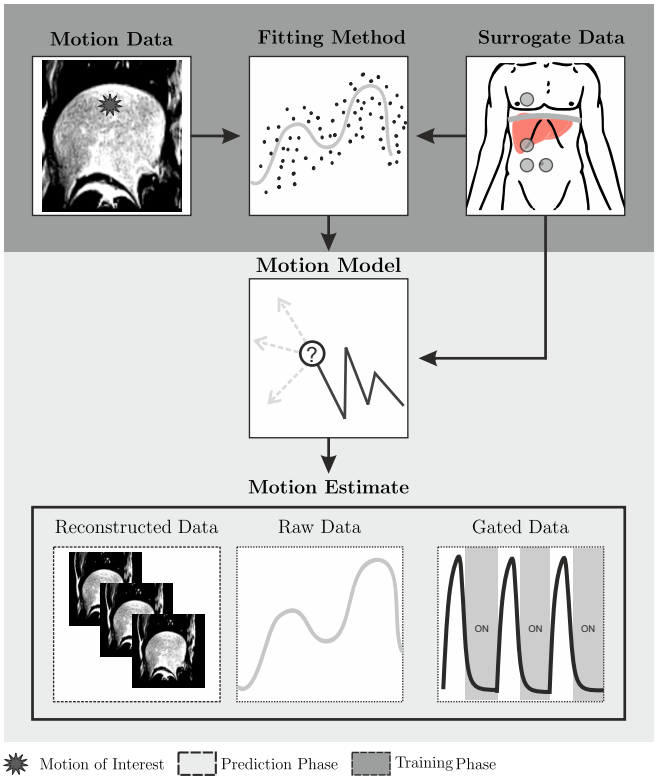

Fig. 2. RME system overview: the figure illustrates the overview of RME. The surrogate data and motion data (which represents the actual internal motion of interest) are acquired at the same time. The fitting algorithm trains the motion model using a supervised learning algorithm such that using only the surrogate data, motion estimates could be predicted.

The system overview and definitions of RME are addressed as follows (see Fig. 2):

- Motion Data: The actual internal motion of interest that are usually medical imaging data acquired at a low update rate [16].
- Surrogate Data: External or internal signals that do not directly measure the internal motion of interest despite having have a strong relationship with the motion data.
- Motion Model: The model is a mathematical description of the relation between the motion data and the surrogate data. The relationship between the surrogate and motion data is represented by set of parameters. For example, if the relationship is linear, the motion data could be estimated by linear combinations of the surrogate data.
- Fitting Method: The method that the motion model uses to fit the surrogate and motion data. This is typically a supervised learning algorithm that computes the parameters of the motion model for the optimal fit.
- Motion Estimate: The motion estimate is the estimated motion determined by the motion model. Usually the motion estimates are reconstructed data of the same type as the motion data. Motion estimates could be of other types, such as raw data (displacements of the internal motion of interest), data of different imaging modality or a boolean gate signal used during respiratory gating.

As shown in Fig. 2, the RME approach consists of two main phases. Firstly, a training phase is required such that the motion data and surrogate data are used by the fitting method to train the parameters of the motion model. Typically, a suitable supervised learning algorithm should be chosen to find the correlation between both data. Secondly, during the prediction phase, the surrogate data (of high update rate) is fed to the motion model and motion estimates are determined.

D. Objectives

This context will be focusing on RME of the liver. The motion data are MRI acquired liver scans while the motion estimates are raw data of the estimated liver motion. The objectives of this paper are summarized as follows:

- Choosing appropriate surrogate data that fit(s) the challenging MR environment.
- Choosing appropriate fitting algorithm(s) that have a strong correspondence between the surrogate and motion data.
- Validating and assessing the designed motion model(s) and the suggested RME framework by conducting human subject experiments.

E. Contribution

Sect. II analyzed and reviewed the various types of surrogate data used in RME. Accordingly, abdominal motion tracking using external markers was chosen as the surrogate data. To the authors' best knowledge, RME of the liver using MRI acquisition is not often addressed in the literature due to its challenging environment. In fact, as shown in Table I, most of the approaches in RME of the liver focus on other types of surrogate data (such as MRI, bellows, accelerometers, etc.). As illustrated in Table I, and to the authors' knowledge, this context is the first in representing RME of the liver using abdominal motion as a surrogate. In the same context, apart from not using MRI as motion data, studies who used external markers as a surrogate for RME of the liver validated their approaches on either phantoms or animal subjects. In fact, the authors paced ahead by extending and validating the suggested approach on human subjects by utilizing state of the art supervised learning fitting methods (namely linear, Ridge and Lasso), and surpassing other studies in RME of the liver by introducing Lasso regression as a fitting method (as shown in Table I).

F. Outline of this Paper

The outline of this paper is as follows. Firstly, the types of the surrogate data are mentioned in Sect. II. In the same section, abdominal motion tracking will be chosen and justified as the optimal surrogate choice during MRI acquisition. Additionally, the designed motion models are presented in Sect. III. The conducted human subjects experiments are presented in details in Sect. IV-C followed by the post-processing methodology in Sect. IV-D. Finally, the results are presented in Sect. V and discussed in Sect. VI followed by the conclusion in Sect. VII.

II. Surrogate Data

A. System Requirements

As explained earlier in Sect. I-D, MRI is the medical imaging modality used. The surrogate data will be selected as follows:

- The surrogates should be MRI compatible such that nether the quality of the MRI acquisition nor the surrogate signal is affected.
- The surrogates should operate safely in the MRI as well as operating outside the MRI.
- The surrogates should not cause additional discomfort or burden to the patient.
- The surrogates should have an enough update rate to capture the variety of the breathing patterns. The update rate should be greater than double the breathing frequency. Thus, since normal breathing is below 0.33 Hz [12], the surrogate update rate should be greater than 0.67 Hz. Additionally, the surrogates should also be high enough to account for processing and computational costs during estimation.

B. Surrogate Data: Analysis

MR navigators are the most common surrogates for MR imaging in RME. They are partial MRI data (window) obtained during acquisition [24]. They are mostly used to track a window of the diaphragm SI motion [13]. The navigators are convenient for MR applications since they do not require extra equipment or installation. However, MR navigators will increase the acquisition time [7]. Moreover, since MR navigators rely on MRI acquisition, they can not be used without the MRI.

Another surrogate example for RME is spirometery. Spirometers reply on measuring the respiratory volume of the air flow in and out of the lungs [25]. The main advantage of spirometers is that they are simple one dimensional signals that have a high correlation to the respiratory motion [26]. However, studies have shown that spirometers have a noticeable drift due to air leakage [24], [27], [28]. as well as a noticeable discomfort for patients [25].

In the same context, respiratory bellows (pneumatic belts) are as common as spirometers. The respiratory bellow is an air filled bag that is tapered around the subject's thorax measuring the thorax motion due to respiration [29]. As the thorax moves due to respiration, air is driven in and out of the bellow creating a flow that is measured [13], [30]. The bellows share the same advantages and disadvantage of spirometers. The most common disadvantage in bellows is in its placement since they restrict the operating area of the patient. Moreover, to get an accurate measurement, the bellows have to be tightly stretched around the patient's thorax, which is uncomfortable for the patient [24].

Accelerometers are also utilized as surrogate signals [31] during percutaneous interventions [5] and have been tested for their MRI compatibility [24]. Nevertheless, they are usually not preferred due to their poor MRI compatibility and low correlation to respiratory motion. [31].

TABLE I

SUMMARY OF THE RELATED WORK ON RESPIRATORY MOTION ESTIMATION (RME) OF THE LIVER.

Related Work	Motion Data	Surrogate Data	Fitting Methods	Experimental Validation
Beddar et al., 2007 [17]	CT	External Markers	Linear Regression	Human Subjects
Odille et al., 2008 [18]	MRI	Respiratory Bellows	Others	Motion Phantom & Human Subjects
White et al., 2009 [19]	MRI	MRI	Others	Human Subjects
Nguyen et al., 2009 [20]	CT	MRI	Others	Human Subjects
Hinkle et al., 2009 [21]	CT	External Markers	Others	Motion Phantom
Ernst et al., 2009 [16]	Xray	External Markers	Support Vector Regression	Porcine Subject
Rijkhorst et al., 2011 [22]	MRI	MRI	Linear Regression	Human Subjects
Buerger et al., 2012 [23]	MRI	MRI	B-spline Smoothing	Human Subjects
Preiswerk et al., 2016 [7]	MRI	US	Kernel Smoothing	Human Subjects
Chen et al., 2017 [24]	MRI	Accelerometers & Bellows	Linear & Ridge Regression	Motion Phantom & Human Subjects
Abayazid et al., 2017 [5]	EM[1]	Accelerometer	RAkEL[2]	Motion Phantom
Fahmi et al., 2017	MRI	External Markers	Linear, Ridge & Lasso Regression	Human Subjects

[1] Electromagnetic sensor [2] Random k-Labelset

Surrogates could also rely on other medical imaging modalities. For example, a low resolution US has been studied to measure the diaphragm motion while using high resolution MRI as motion data [7]. The results are promising, however, US is still not MRI compatible unless the US is wired with optical fibers which might be expensive and fragile. Fluoroscopy could be also used as a real time surrogate for diaphragm tracking. However, it causes additional radiation to the patient [26].

Finally, optical tracking is another choice of surrogate data. By using an infrared (IR) or a digital camera, markers placed on the patient's chest or abdomen are tracked. Many studies showed that tracking the patient's thorax motion by placing external markers has a good correlation with respiration [16], [17], [25], [31] - [32]. For example, Beddar et al. used Real-time Position Management System (RPM, Varian Medical Systems, Palo Alto, CA) which had a reflective marker placed on the human's abdomen and tracked using IR camera [17]. Beddar et al. also showed that the motion is well correlated with the internal motion of liver [17]. Vedam et al. studied the same effect but for internal motion of the diaphragm and obtained similar correlation results [33] . Moreover, Ernst et al. studied the correlation between multiple external IR reflective LEDs and the internal liver motion of a swine in which it was shown that one marker was not sufficient for tracking the liver motion [16]. Henningsson et al. and Wasza et al. stated that using external markers is advantageous due to its high temporal and spacial resolution [30], [34]. Wilms et al. also elaborated that by using optical tracking, multiple markers could be advantageous since the dimensionality of the system will increase without adding an extra cost to the setup [35].

C. Surrogate Data: Selection

Optical tracking is the final choice for the surrogates. Using MR navigators is not preferred since it depends on MRI acquisition thus would not operate without MRI. Accelerometers are also not preferred due to its limited MRI compatibility. Spirometers and bellows are rejected due to their lack of information, discomfort to the patient and due to the limited space of the MRI environment. As a result, optical tracking is the optimal choice for the following reasons:

- They are Image modality independent such that they could be used with and without MRI.
- They are not tighten around the patient's abdomen but stuck on the body and thus saving space.
- They are drift free [36].
- They are not one dimensional since multiple markers could be placed in different locations.

An industrial color camera is chosen compared to infrared due to is relatively cheaper cost and availability. IR tracking is less sensitive to light intensities. However, the light environment of the MRI room does not change dramatically to choose IR instead.

III. MOTION MODEL

A. Motion Model: Analysis

According to [13], the motion model is made up of the following:

- Choice of surrogate data: What are the types of surrogates used? As explained earlier in Sect. II-C, optical tracking of multiple markers are the chosen surrogate data.
- Choice of motion representation: How is the motion represented in the model? In this context, the liver motion is presented by the SI displacement of the liver upper border and the abdominal motion is represented by the tracked displacements of the markers.
- Motion model correspondence: How it the motion data related to the surrogate data? If the model is patient and session specific (intra-fractional variation, which is the case in this context), linear representations are sufficient. Linear representation does not mean using a single 1D surrogate, but means that the motion model could be estimated by linear combinations of the surrogates.

- Fitting method: Which algorithm is chosen to fit the data motion model? Since the motion and surrogate data are linearly related, linear fitting methods were chosen in this context. The most common method is multivariate linear regression (MVR) [13], [37]. Other methods are modifications of MVR such as Ridge regression [38], [39], principle component regression [40], etc.

Given that the liver motion could be estimated by linear combinations of the tracked markers, MVR was used as a fitting method. Shrinkage methods (such as Ridge and Lasso) were also used and compared to MVR. Shrinkage methods are used when multiple surrogate data that are highly correlated with each other are used.

B. Multivariate Linear Regression (MVR)

The main objective of MVR is, given a set of N training sample pairs $\{(x_1, y_1), (x_2, y_2), ..., (x_N, y_N)\}$, find (learn) a regression model $f(x)$ that could predict new values of y. The MVR model $f(x_i)$, for a sample pair (x_i, y_i) is formulated as follows:

$$y_i \approx f(x_i) = \beta_0 x_{i0} + \sum_{j=1}^{p} x_{ij}\beta_j \tag{1}$$

such that $\beta = [\beta_0, \beta_1, ..., \beta_p]$ are the parameters/coefficients of the regression model, $x_i = [x_{i1}, x_{i2}, ..., x_{ip}]$ are the model features of the ith sample, p is the number of parameters. x_{i0} is a dummy unity variable called the intercept. Under the assumption that y could be estimated from linear combinations of the features, the parameters β are estimated using the ordinary least squares (OLS) method [37]. The parameters β are obtained by minimizing the cost function $J(\beta)$ over all the training samples:

$$\begin{aligned} J(\beta) &= \sum_{i=1}^{N}(y_i - f(x_i))^2 \\ &= \sum_{i=1}^{N}(y_i - \beta_0 x_{i0} - \sum_{j=1}^{p} x_{ij}\beta_j)^2 \end{aligned} \tag{2}$$

The optimization problem is solved either analytically using the normal equation or numerically using the gradient descent. In this context, y represents the liver motion acquired from the motion data while x represents the markers motion acquired from the surrogate data.

C. Shrinkage Methods

MVR obtains a set of parameters β that minimizes the cost function $J(\beta)$ to obtain the optimal fit to the training samples (training data). However, MVR could be challenging when dealing with multiple features because overfitting might happen since the grater the number of features, the more MVR tries to fit the training data[37]. Moreover, the training data might contain noise or idiosyncratic characteristics. Thus, the more the features the more MVR captures the noise of the signal rather than the physical model. Overfitting might also occur when the features are highly correlated which is the case when the features are tracked markers locations [13]. As a result, MVR has to be extended to penalize the model for the number of parameters β [41]. One of the shrinkage methods is Ridge regression [42]. Ridge regression extends the cost function of MVR such that the cost function is written as follows:

$$\begin{aligned} J_R(\beta) &= \sum_{i=1}^{N}(y_i - \beta_0 x_{i0} - \sum_{j=1}^{p} x_{ij}\beta_j)^2 + \lambda\sum_{j=1}^{p}\beta_j^2 \\ &= \underbrace{J(\beta)}_{\text{Fitting Penalty}} + \underbrace{\lambda\sum_{j=1}^{p}\beta_j^2}_{\text{Shrinkage Penalty}} \end{aligned} \tag{3}$$

Thus, in Ridge regression, we penalize the model for the number of coefficients by tuning the shrinkage parameter λ ($\lambda \geq 0$). If λ is zero then we're back in MVR. If λ is too big then the model is optimized to minimize the parameters rather than fitting the model which will underfit the data. The greater the shrinkage parameter, the more the parameter β shrinks towards zero. Thus, there has to be a trade off in selecting the shrinkage coefficient. The parameter λ is tuned by validating the motion model over a set of validation data and choosing the parameter λ which results in the smallest prediction error. Shrinkage parameter selection is stated in Sect. III-E.

Lasso regression is another method for shrinking the regression parameters [43]. However, unlike Ridge, Lasso penalizes the absolute size of the coefficients as follows:

$$J_L(\beta) = \underbrace{J(\beta)}_{\text{Fitting Penalty}} + \underbrace{\lambda\sum_{j=1}^{p}|\beta_j|}_{\text{Shrinkage Penalty}} \tag{4}$$

The main difference between Ridge and Lasso is that Ridge shrinks the parameters towards zero while Lasso has the ability to shrink the parameters to exactly equal to zero [41]. This means the the corresponding feature is neglected, if the shrinkage parameter λ is relatively large. Thus, Lasso has the ability to cancel out the features that are not needed. In other words, if the features are highly correlated, Lasso selects number of features and shrinks the others to zero. On the other hand, Lasso is relatively more computationally expensive than Ridge because there is no closed form solution for its optimization problem.

D. Model Selection

The aim of the motion model is to predict future liver motion given a set of training data. Thus, to evaluate the model, it is important to know how will the model perform upon new dataset (so called test data) which means that we are interested in knowing the test error rather than training error. In other words, evaluating the model based on the training data alone will result in giving optimistic values that might not be the same if new dataset are used. Moreover, the features and shrinkage parameter should be also selected based on another set of data (so called validation data). Accordingly, the acquired dataset has to be split into three segments: training data, validation data and

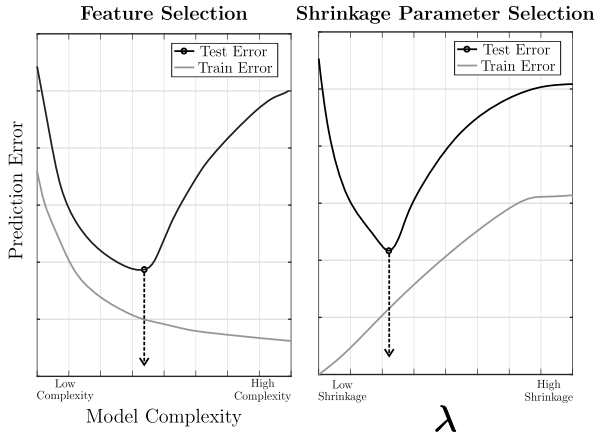

Fig. 3. Feature and Shrinkage Parameter Selection: the figure represents the procedure to select the features (left) and shrinkage parameter λ (right) for the chosen regression algorithms. The figure also shows that the selection should be based on the validation data.

test data [37]. Such that the training data is used to fit the models, the validation data is used to select the features and shrinkage parameter and the test data is used to evaluate the performance of the models. The ratio between the test, selection and training data are chosen to be 50%, 20% and 30% respectively.

E. Feature and Shrinkage Parameter Selection

The features are selected such that they are simple, interpretable, intuitive and have a good fit to the data. The types of the features could be designed as follows [37]:

- Quantitative: Numeric values of the input signals such as the positions of the markers.
- Basis Expansions: Polynomial representations of the input signals (quadratic, cubic, or higher order representations).
- Others: In the context of RME, it could be the derivative(s) of the input signals [5], [16] or a signal indicating inhalation/exhalation [13], or a signal indicating the respiratory phase.

It is important to note that the number of features selected affects the overall fit of the data. It is not preferred to use many unnecessary features which might cause overfit. Moreover, MVR is scale invariant, which means that the scale of the features does not matter. However, since in shrinkage methods, the cost function penalizes the sum of the parameters, the parameters should have the same scale [41]. Thus, after selecting the types of features, the features are scaled to have a common scale range. The features are normalized to have approximately a zero mean and unit standard deviation.

Additionally, after choosing the regression algorithm, the features should be selected. As shown in Fig. 3, features should be selected based upon the validation data because the higher the model complexity the lower the training error (since the higher the complexity of the model the more the model tries to overfit the data) is which is not intuitive. Thus, by using the validation data, a minimum value will correspond to the optimal feature type. In the same context, the shrinkage parameter will be selected by varying the shrinkage parameter and selecting the one with the lowest prediction error. The lower the shrinkage parameter, the smaller the value of λ. As shown in Fig. 3, the shrinkage parameter should also be selected based upon the validation data.

F. Model Evaluation

To evaluate the models used, two performance measures will be calculated. These performance measures are the mean absolute error (MAE) and the adjusted coefficient of determination (adjusted R squared, $\mathrm{R}^2_{\mathrm{adj}}$) and are calculated as follows:

$$\mathrm{MAE} = \frac{\sum_{i=1}^{N} |Y_i - \hat{Y}_i|}{N} \tag{5}$$

$$\mathrm{R}^2_{\mathrm{adj}} = 1 - \frac{\mathrm{RSS}.(n-1)}{\mathrm{TSS}.(n-k)} \tag{6}$$

such that N is the number of test samples and k is the number of predictors (β) including the intercept (which could also be interpreted as the number of features). Y_i and $\hat{Y}_i$ are the actual (ground truth) and estimated liver motion from the test data respectively. Moreover, RSS and TSS are the residual and total sum of squares respectively and calculated as follows:

$$\mathrm{RSS} = \sum_{i=1}^{N} (Y_i - \hat{Y}_i)^2 \tag{7}$$

$$\mathrm{TSS} = \sum_{i=1}^{N} (Y_i - \bar{Y})^2 \tag{8}$$

such that $\bar{Y}$ is the mean value of Y. Note that $\mathrm{R}^2_{\mathrm{adj}}$ is an indication of the goodness of the fit of the model. $\mathrm{R}^2_{\mathrm{adj}}$ could be any value less than or equal 1. $\mathrm{R}^2_{\mathrm{adj}}$ closer to 1 indicates a better fit. $\mathrm{R}^2_{\mathrm{adj}}$ is used compared to R^2 because the former pays an extra price for the inclusion of unnecessary features [41]. Furthermore, MAE is used to obtain a quantitative result of the predicted response. The smaller the MAE the smaller is the test error.

IV. Experiments

A. Overview

The previous sections presented an overview of the suggested RME system such that the motion data was presented as MRI acquired liver scans while the surrogate data were presented as tracked abdominal motion using a digital camera. Moreover, MVR, Ridge and Lasso were chosen as motion models. In this section, the suggested approach was validated by conducting human subject experiments. Fig. 4 presents an overview of the experimental setup such that the presented study involved two markers placed on the subject's abdomen tracked using a digital camera outside the MRI cage. A regular MRI coil was placed on the subject's thorax away from the markers to acquire MRI liver scans. The surrogate and motion data were acquired simultaneously at different update rates.

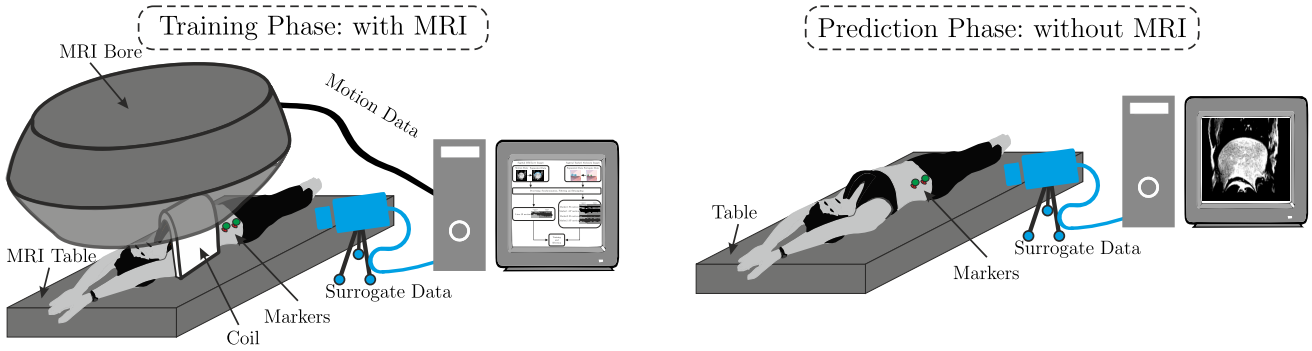

Fig. 4. Overview of the experimental setup. Firstly, during the training phase, the motion and surrogate data are acquired simultaneously. Moreover, during the prediction phase, based solely on the surrogate data, the motion estimate are predicted.

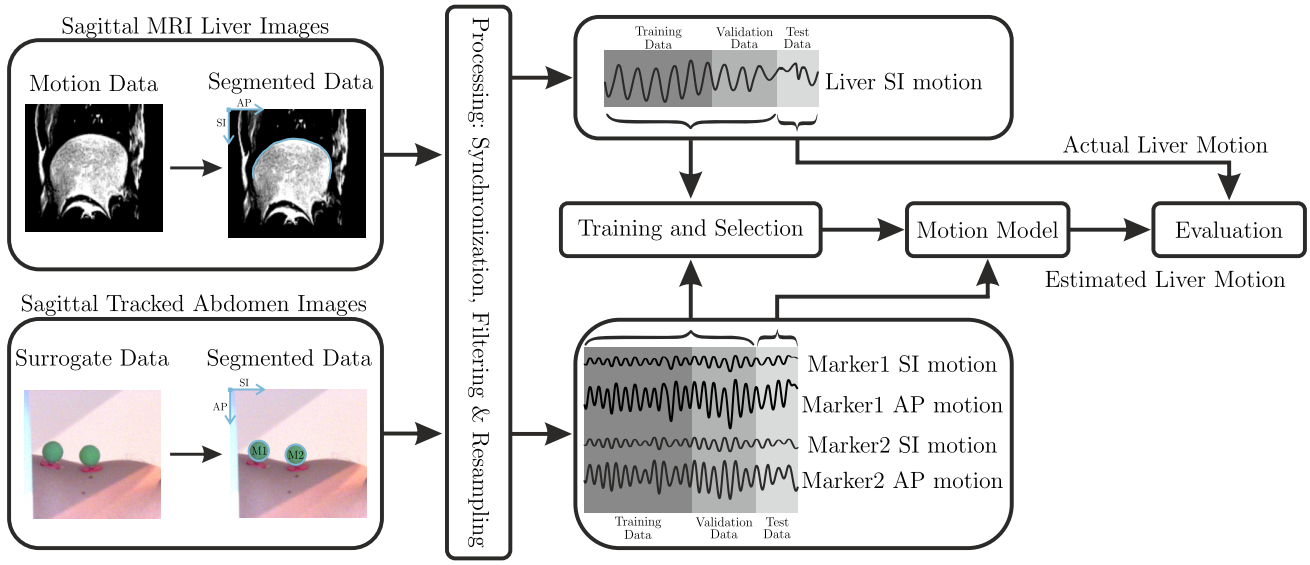

Fig. 5. Workflow of the suggested approach. Firstly, the sagittal MRI liver images and camera acquired abdominal motion were acquired simultaneously. The acquired images were segmented and the liver and marker motion were extracted. Additionally, the acquired data are processed and split for designing and evaluating the motion model.

Subsequently, the three motion models were trained offline. In the actual scenario, the subject should be requested to leave the MRI and based solely on the tracked abdominal motion, the motion data are estimated. However, since evaluating the motion estimate required the knowledge of the true values of the motion data, the subject did not leave the MRI room.

B. Workflow

The workflow of the proposed approach is shown in Fig. 5. Firstly, the motion and surrogate data were acquired simultaneously with their relative timestamps. Additionally, the MRI and camera images were segmented offline and the liver and abdominal motion were extracted. Moreover, the extracted signals were processed and split into three datasets (training, validation and test data). The training and validation data were utilized to train the motion model while the test data of the abdominal motion was fed to the motion model. The motion model estimated the liver motion and therefore was evaluated compared to the actual liver motion.

C. Human Subject Experiment

1) Measurement Protocol: Three healthy subjects (two males and one female) over the age of 18 participated in the human subject experiments. Each subject was informed about the study, received a detailed description of the experiment and filled in a consent form. The investigators made sure that the subjects were familiar with MRI safety regulations. Each subject was subjected to two sessions, 3 minutes each. The total investment time of each subject was 60 minutes (including the two sessions, pre- and post- scan procedures). The experiments were done at the University of Twente (Enschede, the Netherlands) and an ethical proposal have been approved by the local medical ethical committee of the university. During the scan, each subject was requested to breath normally (without any previous training) and try not to move during the scan. For more details regarding the measurement protocol and the consent form of the human subject experiments, refer to Appendix[A,B] respectively.

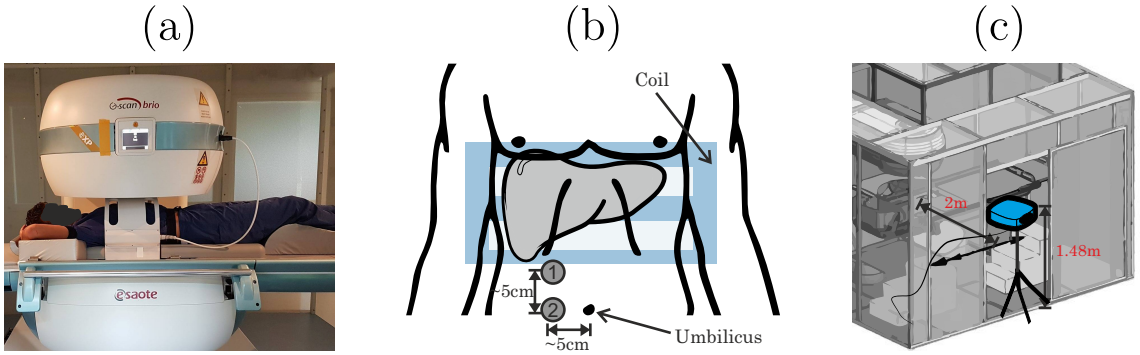

Fig. 6. Hardware Setup: (a) Subject is positioned in supine position with his/her hands behind the head. A suitable coil was adjusted such that the subject's liver is centered. Head, elbow, back and feet cushions were added for the subject's comfort. (b) Two markers were placed on the subject's abdomen. Preliminary experiments were conducted to determine the optimal marker locations. The markers are placed 5cm to the right of the subject's umbilicus. Marker M2 is coinciding horizontally from the subject's umbilicus and marker M1 is 5cm above M2. (c) The camera is placed at the door of the MRI cage which is approximately 2m from the center of the MRI bore facing the subject's sagittal plane.

2) Hardware Setup: The setup consisted of two main modalities: MRI and camera tracking. The MRI system used was the ESAOTE© G-scan Brio system (Genoa, Italy) which is a 0.25 T open-bore MRI system (as shown in Fig. 6a). The MRI system is at the University of Twente. As shown in Fig. 6a, the subject was placed on the MRI table in supine motion with the head is to the left of the MRI system. Additionally, the subject was positioned with his/her hands behind his/her head. A suitable coil was positioned such that the center of the field of view is approximately at the border of the liver. Accordingly, an initial placement of the subject required moving towards the coil till the subject's armpit reached the coil. Further subject positioning was performed to obtain an optimal field of view for the liver (see Appendix[A]).

Two 2 cm diameter 3D printed markers were placed on the subject's abdomen as shown in Fig. 6b. These marker locations were chosen during preliminary experiments (in Sect. V-A). The marker locations were chosen to have the largest excursion (range) of the abdomen. As shown in Fig. 6b, the markers were placed 5 cm to the right of the subject's umbilicus such that the first marker was placed 5 cm above the second marker. Both markers were placed away from the MRI coil.

An industrial camera (MVBlueFox3) from Matrix Vision© (Oppenweiler, Germany) was chosen with a suitable lens (25 mm, 1.4 focal length) to track the subject's chest. The camera was placed outside the MRI cage (approximately 2 m from the center of the MRI bore) facing the subject's sagittal plane (as presented in Fig. 6c).

3) Data Acquisition: For the MRI acquisition, a predefined sequence from ESAOTE© G-scan Brio was performed. The MRI sequence is a 0° 2DHYCES, sagittal plane, slice thickness = 15 mm, repetition time = 7 s, echo time = 3.5 s, reconstructed resolution = 1.5 mm × 1.5 mm, flip angle = 40°, field of view = 38 mm × 38 mm, temporal resolution approximately 1 fps. The markers were acquired at 10 fps with a spacial resolution of 0.15 mm. The region of interested of the camera was 200 mm × 200 mm. The time stamp of each acquired frame from the MRI and the camera was recorded for temporal alignment and synchronization.

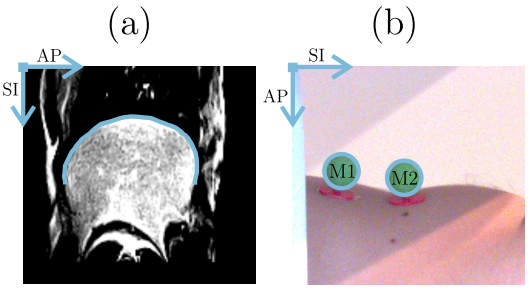

Fig. 7. Post-processing: the figure represents the acquired frames from MRI and camera and the segmented output. The markers were segmented from the camera while the liver's border was segmented from the MRI. The corresponding superior-inferior (SI) and anterior-posterior (AP) axes of the markers and the liver are presented at each segmented frames. According to the defined frames, inhalation corresponds to a negative SI and AP for the markers and positive SI and AP for the liver.

D. Post-processing

1) Image Processing: Consequently, after MRI and camera acquisition, the video streams were segmented. Each DICOM frame from the MRI video stream (with its relative time stamp) was segmented using a suitable threshold value. Series of morphological operations (erosion, dilation and edge detection) were performed to detect the upper border of the liver. Only the SI motion was detected due to the fact that the acquired spacial resolution (1.5 mm × 1.5 mm) was too low to detect the respiratory induced AP motion (which is approximately 2 mm [8]). The segmented SI positions were computed relative to the reference frame as shown in Fig. 7a.

In a similar manner, each frame from the camera video stream (with its relative time stamp) was segmented using a suitable threshold value (as shown in Fig. 7b). Series of morphological operations were performed to detect the markers. The markers' SI and AP centroid positions are computed relative to their relative frame. As shown in Fig. 7, inhalation corresponds to a negative SI and AP marker motion and positive SI and AP liver motion (and vice versa).

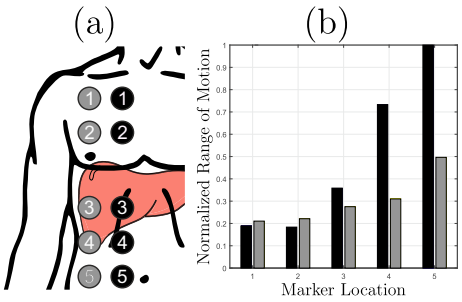

Fig. 8. Marker Location: Fig. 8(a) represents different marker locations and their corresponding normalized range of motion in Fig. 8(b). The figure shows that markers 4 and 5 have the higher range of motion compared to the other markers. The figure also shows that the closer the markers are from the umbilicus, the higher the range of motion.

2) Signal Processing: After image segmentation, the markers' positions (SI and AP positions of the two markers) and the liver's SI position were processed. First, outliers were observed manually and omitted from the signals. Moreover, a suitable low pass filter was designed for the two signals. The signals were re-sampled in order to obtain the same sample rate. Finally, the signals were transformed from pixel dimensions into millimeter dimensions by multiplying each signal with its calibrated pixel spacing (1.5 mm and 0.15 mm for the MRI and camera acquired frames respectively). Temporal synchronization was performed in two steps. Firstly, the two signals were aligned according to their relative time stamps. Secondly, the two signals were aligned using correlation analysis to correct for the time delay.

V. Results

This section presents the evaluation and validation of the RME of the liver with abdominal motion as a surrogate. Firstly, a preliminarily experiment conducted to investigate the optimal marker location is presented in Sect. V-A. The analysis of the acquired MRI and camera signals (including power density, correlation and motion analysis) are presented in Sect. V-B to Sect. V-D. Furthermore, the features selection and shrinkage parameters tuning of the motion models are demonstrated in Sect. V-E and Sect. V-F respectively. Finally, the estimated SI motion of the liver is compared to the actual SI motion and is presented in Sect. V-G.

A. Marker Locations

To select the optimal marker location, a preliminary experiment was conducted to track the markers in several locations. Fig. 8a represents the markers in several locations and their corresponding normalized range of motion in Fig. 8b. The markers' locations were chosen to have the highest range of motion (excursion). As shown in the Fig. 8, the range of motion increased ascendingly from marker location 1 to 5. Marker locations 4 and 5 showed the highest range of motion compared to the other marker locations. Moreover, the closer the marker was to the subject's umbilicus, the higher the range of motion. However, during camera tracking, it was preferred to locate the markers away from the center of the MRI bore to avoid any shadow

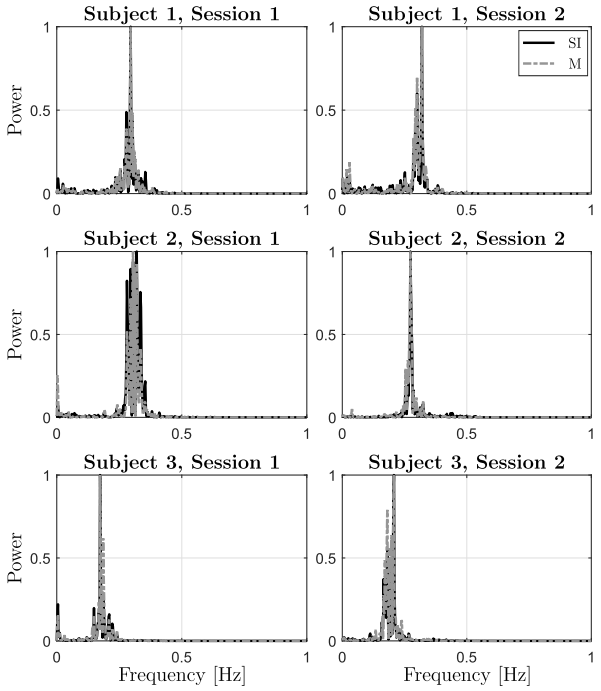

Fig. 9. Power Density Analysis: the figure shows the power density (periodogram) of the liver superior-inferior (SI) motion (black solid line) and the markers motion (gray dotted line) for all the subjects. The figure shows that the signals are dominated by breathing frequencies below (0.5 Hz). However, there are spikes in the low frequencies (below 0.1 Hz). The figure also shows no heart beat induced motion

or inconsistent light conditions. Thus, a trade off has been chosen and markers 4 and 5 were chosen to be in the midway between the two vertical locations to the right of the umbilicus as explained in Sect. IV-C.2.

B. Power Density Analysis

Fig. 9 represents the normalized power density of the markers and the liver (SI) signals for all the sessions. Comparing the plots in the same row allows the assessment of intrafractional variations between patients while the columns allow the assessment of the variations between patients. As shown in the figure, the liver and marker signals were dominated by the breathing frequencies [12]. The figure also represented spikes at low frequencies (smaller than 0.1 Hz) which indicated the presence of noise or drift in positions. The figure also showed that each subject had a different breathing pattern thus the model has to be patient specific. Moreover, Fig. 9 showed that the breathing patterns are not identical for each subject over the two sessions which clearly confirmed that the model should be updated for the each session (intrafractionally). Note that according to the obtained data, the signals were not affected by other organ induced motion such as the heart beats (operating over 1 Hz [12]). This is because for the MRI acquired liver signals, the temporal resolution (1 fps) would not capture such high frequencies. However, for the markers, even though the temporal resolution would capture heart beats, the markers signals were not affected by the beats due to the fact that the markers were located away from the heart.

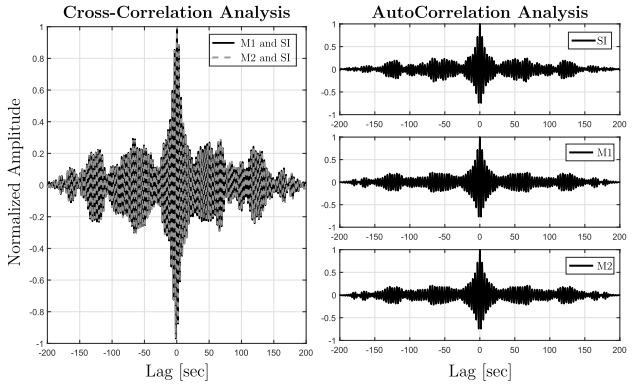

Fig. 10. Correlation Analysis: The figure shows the auto correlation (right) and cross correlation (left) analysis of the liver SI motion and the two markers M1 and M2. The figure shows that the signals are not rhythmic and well synchronized.

C. Correlation Analysis

Fig. 10 represents the normalized auto correlation (of the liver SI motion and markers M1 and M2) and cross correlation (of the liver SI motion and M1 and the liver SI motion and M2) of the signals. The cross correlation analysis showed that the signals are not rhythmic (which was expected since breathing signals varies at different respiratory cycles). Moreover, the cross correlation plots showed that both signals are temporally aligned with no observed time delay between the liver and markers motion.

D. Motion and Surrogate Data Analysis

Fig. 11 represents the processed data of the subjects. The figure presents the mean and the standard deviation ($\mu \pm \sigma$) of the peak-to-trough (PPT) motion of the liver SI motion and the markers SI and AP motion. As shown in Fig. 11, the motion data showed expected range of motion [8]. Subject 3 had the highest range of motion for the liver and abdominal motion. The other two subjects had approximately similar range of motion. The values of the curves plotted in Fig. 11 are summarized in Table II. As shown in Table II, the highest PTT liver and markers motion were observed in subject 3. The maximum PTT motion was 21.3 mm for the liver's SI motion, 13.9 mm and 11.7 mm for the two markers' AP motion and 1.9 mm and 3.2 mm for the two markers' SI motion (all observed in subject 3). The minimum PTT motion was 10.0 mm for the liver's SI motion (observed in subject 1), 0.4 mm and 0.2 mm for the two markers' SI motion (observed in subjects 1 and 2 respectively) and 2.5 mm for the two marker's AP motion (observed in subject 2). In all subjects, the markers' AP motion had a higher range of motion than their SI motion. The tables also demonstrated the variations in breathing magnitudes between the subjects and between each session thus confirming that the motion models should be patient specific.

E. Feature Selection Analysis

Nine types of features have been chosen as shown in Table III. In order to chose the optimal feature type, each feature type was validated using the validation data as explained in Sect. III-E and Fig. 3. Moreover, Fig. 12 represents the normalized MAE (NMAE) against the type of feature for the training and validation data. The type of feature is directly proportional to the model complexity. Thus, the higher the feature type the higher the model order and thus the complexity. As shown in Fig. 12, choosing more than one marker improved the estimation accuracy. However, marker 2 (type 2) outperformed marker 1 (type 1). Moreover, choosing a more complex model (higher order) did not improve the performance of the model upon new data (test data). Thus, the optimal feature selected was type 3. Finally, Fig. 12 also demonstrated that the type of feature should be selected upon validated data and not training data.

F. Shrinkage Parameter Analysis

The shrinkage parameters (for Lasso and Ridge) were selected by validating the model performance using the validation data. Ridge and Lasso models had the same type of feature selected in Sect. V-E. Fig. 13 represents the NMAE against the shrinkage parameter λ for Ridge and Lasso. Fig. 13 showed expected results as explained in Sect. III-E and Fig. 3. However, due to the limited resolution acquired for the liver data, the feature and shrinkage analysis were more challenging to tune. According to Fig. 13, the shrinkage parameter was minimal at the values $(0, 0.2]$ and $(0, 0.4]$ for Ridge and Lasso respectively. Thus, the average values of λ were taken. These values were 0.1 and 0.2 for the Ridge and Lasso algorithms respectively.

G. Estimation Accuracy

This subsection is evaluating the performance of the designed motion models. To evaluate the designed models, the estimated liver SI motion $\hat{Y}$ obtained from the regression model in (1) was compared t0 the true values of the liver SI motion Y. The three fitting methods used were MVR, Ridge and Lasso. Feature type 3 was chosen for the three methods and the chosen shrinkage parameter λ was 0.1 and 0.2 for Ridge and Lasso respectively.

Fig. 14 represents the plots of the estimated $\hat{Y}$ and the true values Y of the liver SI motion using the test data acquired from the conducted six sessions using MVR, Ridge and Lasso. Each row in Fig. 14 corresponds to one session. Thus, comparing the plots in the same row allows the assessment of the three designed models while comparing the plots in the same column allows the assessment of each regression model through out the sessions. Tables IV and V represent the performance measures (MAE and $\mathrm{R}^2_{\mathrm{adj}}$ respectively) of the estimated liver SI motion using MVR, Ridge and Lasso. The performance measures MAE and $\mathrm{R}^2_{\mathrm{adj}}$ are calculated for each session. Furthermore, each row in IV and V correspond to one session. Thus, comparing the values in the same row allows the assessment of the three designed models while comparing the values in the same column allows the assessment of each regression model through out the sessions. As mentioned earlier in Sect. III-F, $\mathrm{R}^2_{\mathrm{adj}}$ closer to 1 indicates a better fit while MAE closer to 0 indicates a better estimation accuracy.

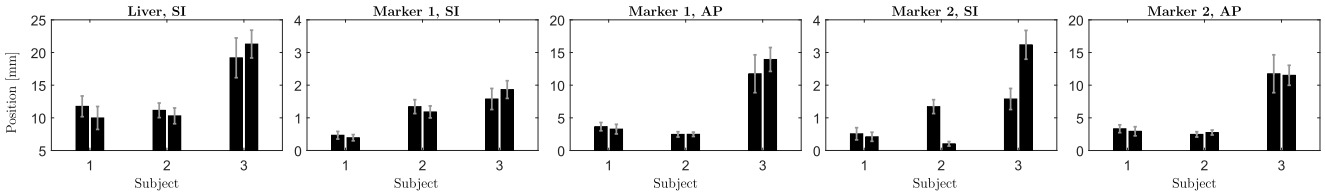

Fig. 11. Motion Data Analysis: mean μ and standard deviation σ of peak-to-trough (PTT) motion of the liver's SI motion and the markers' SI and AP motion. The mean and standard deviation of the presented figure is summarized in Table II.

TABLE II

MOTION DATA ANALYSIS: MEAN μ AND STANDARD DEVIATION σ OF PEAK-TO-TROUGH (PTT) MOTION OF THE LIVER SI MOTION AND THE MARKERS SI AND AP MOTION .

Subject, Session	SI ($\mu \pm \sigma$)	Marker 1, SI ($\mu \pm \sigma$)	Marker 1, AP ($\mu \pm \sigma$)	Marker 2, SI ($\mu \pm \sigma$)	Marker 2, AP ($\mu \pm \sigma$)
Subject 1, Session 1	11.8 $\pm$ 1.6	0.5 $\pm$ 0.1	3.7 $\pm$ 0.6	0.5 $\pm$ 0.2	3.3 $\pm$ 0.6
Subject 1, Session 2	10.0 $\pm$ 1.8	0.4 $\pm$ 0.1	3.3 $\pm$ 0.7	0.4 $\pm$ 0.1	2.9 $\pm$ 0.7
Subject 2, Session 1	11.1 $\pm$ 1.1	1.3 $\pm$ 0.2	2.5 $\pm$ 0.4	1.3 $\pm$ 0.2	2.5 $\pm$ 0.4
Subject 2, Session 2	10.3 $\pm$ 1.2	1.2 $\pm$ 0.2	2.5 $\pm$ 0.3	0.2 $\pm$ 0.1	2.8 $\pm$ 0.4
Subject 3, Session 1	19.2 $\pm$ 3.0	1.6 $\pm$ 0.3	11.7 $\pm$ 2.9	1.6 $\pm$ 0.3	11.7 $\pm$ 2.9
Subject 3, Session 2	21.3 $\pm$ 2.1	1.9 $\pm$ 0.3	13.9 $\pm$ 1.8	3.2 $\pm$ 0.4	11.5 $\pm$ 1.5

TABLE III

FEATURE SELECTION: THE TYPES ARE ARRANGED SUCH THAT THE TYPE 1 CORRESPONDS TO THE LEAST COMPLEX AND TYPE 9 CORRESPONDS TO THE MOST COMPLEX.

Type	Description
Type 1	Marker 1
Type 2	Marker 2
Type 3	Marker 1 and Marker 2, 1st order polynomial
Type 4	Marker 1 and Marker 2, 2nd order polynomial
Type 5	Marker 1 and Marker 2, 3rd order polynomial
Type 6	Marker 1 and Marker 2, 4th order polynomial
Type 7	Marker 1 and Marker 2, 5th order polynomial
Type 8	Marker 1 and Marker 2, 6th order polynomial
Type 9	Marker 1 and Marker 2, 7th order polynomial

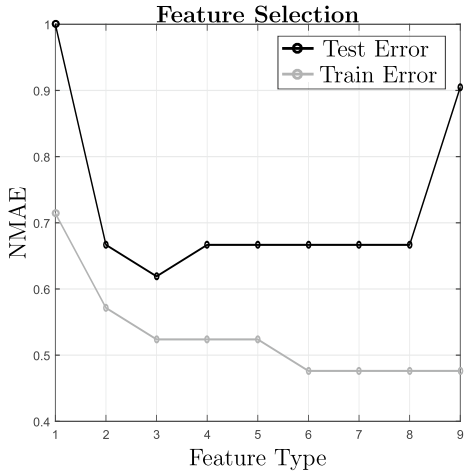

Fig. 12. Feature Selection: the figure represents the normalized MAE (NMAE) against the feature type. The plot shows that feature type # 3 has the smallest NMAE and thus is the selected feature type.

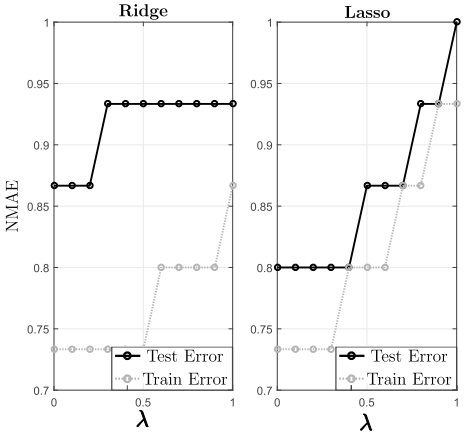

Fig. 13. Shrinkage Parameter Selection: the figure represents the normalized MAE (NMAE) against the shrinkage parameter λ for both Ridge and Lasso regression. The plot shows that the minimum NMAE is at approximately 0.1 for Ridge and 0.2 for Lasso.

As shown in Fig. 14, the three algorithms managed to properly estimate the liver motion. There was no time lag observed between the estimated and the actual plots in the first two subjects. However, subject 3 had an observable deviation in both session during the first 20 seconds. As shown in Table IV, subject 3 had a maximum MAE of 1.9 mm $\pm$ 1.9 mm , 1.8 mm $\pm$ 1.9 mm and 1.8 mm $\pm$ 1.9 mm for MVR, Ridge and Lasso respectively while subject 2 had the minimum MAE of 0.8 mm $\pm$ 0.7 mm for MVR, Ridge and Lasso. For subjects 1 and 2, Lasso generally outperformed MVR and Ridge in the first session while the three models had equal estimation accuracy in the second session (as shown in Table IV). For subject 3, MVR and Lasso had a higher accuracy than Ridge during the first session while Ridge and Lasso had a higher accuracy during the second session. As shown in Table V, Lasso outperformed Ridge and MVR in the first three sessions. The

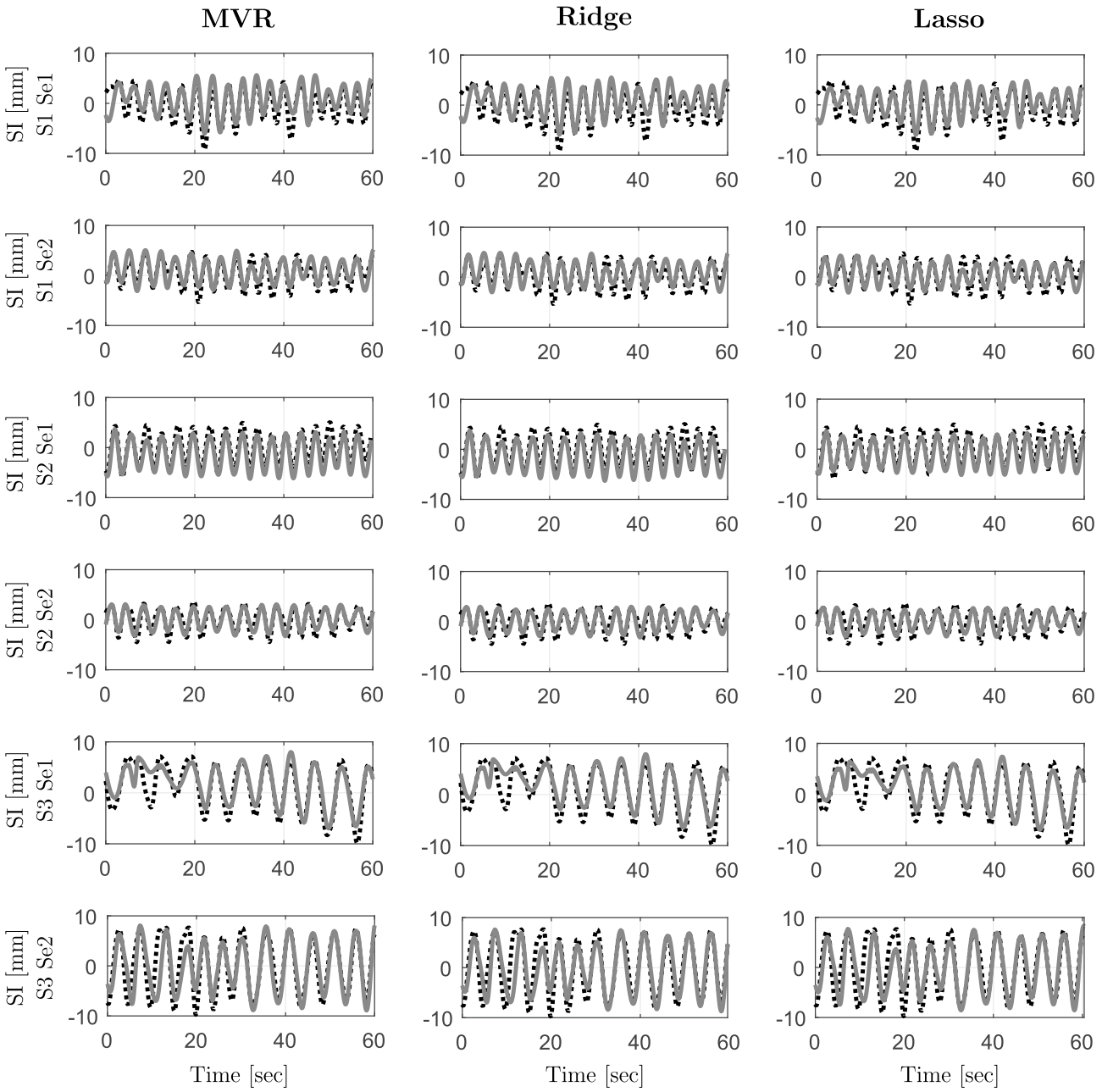

Fig. 14. Evaluation Results: the figure represents the estimated values of the liver SI motion ($\hat{Y}$) compared with the actual liver SI test data Y against time. Each row of the figure represents the subject (S) and session number (Se) while each column represents the regression algorithm used. The MAE, standard deviation and $\mathrm{R}^2_{\mathrm{adj}}$ of the presented graph is summarized in tables IV and V respectively.

second session of the second subject and the first session of the third subject had similar performance by the three models. Finally, Lasso and Ridge outperformed MVR during the second session of the third subject. As a general trend, Lasso outperformed MVR and Ridge in three of the six conducted sessions while in the other three, Lasso had equal performance with Ridge.

VI. Discussion

In the previous section, we evaluated the developed RME approach. A preliminary experiment was conducted to evaluate the optimal marker locations and showed that the closer the marker is from the subject's umbilicus, the higher is the range of motion. These results were shown in Fig. 8 and were validated also in Fig. 12 such that the higher the marker range, the higher the estimation accuracy. The data acquired from the markers and the MRI showed that breathing signals vary between patients and consequently the models designed were patient specific. The acquired data also showed no indication of other induced motion (such as the heart). The liver SI motion ranged between 10.0 mm - 21.3 mm which is consistent with other previous studies on the liver [17], [11]. The markers motion were dominant in

TABLE IV

EVALUATION RESULTS: MAE AND STANDARD DEVIATION σ OF THE ESTIMATED LIVER SI MOTION USING MVR, RIDGE AND LASSO.

	MVR	Ridge	Lasso
Subject, Session	MAE $\pm$ σ	MAE $\pm$ σ	MAE $\pm$ σ
Subject 1, Session 1	1.5 $\pm$ 1.2	1.5 $\pm$ 1.1	1.2 $\pm$ 1.1
Subject 1, Session 2	1.0 $\pm$ 0.8	1.0 $\pm$ 0.7	1.0 $\pm$ 0.7
Subject 2, Session 1	1.4 $\pm$ 0.8	1.4 $\pm$ 0.8	1.0 $\pm$ 0.7
Subject 2, Session 2	0.8 $\pm$ 0.7	0.8 $\pm$ 0.7	0.8 $\pm$ 0.7
Subject 3, Session 1	1.5 $\pm$ 1.3	1.6 $\pm$ 1.3	1.5 $\pm$ 1.2
Subject 3, Session 2	1.9 $\pm$ 1.9	1.8 $\pm$ 1.9	1.8 $\pm$ 1.9

TABLE V

EVALUATION RESULTS: R^2_{adj} OF THE ESTIMATED LIVER SI MOTION USING MVR, RIDGE AND LASSO.

	MVR	Ridge	Lasso
Subject, Session	R^2_{adj}	R^2_{adj}	R^2_{adj}
Subject 1, Session 1	0.6	0.6	0.7
Subject 1, Session 2	0.7	0.7	0.8
Subject 2, Session 1	0.7	0.7	0.8
Subject 2, Session 2	0.8	0.8	0.8
Subject 3, Session 1	0.8	0.8	0.8
Subject 3, Session 2	0.7	0.8	0.8

the AP (ranged between 2.5 mm - 13.9 mm) rather than the SI motion (ranged between 0.2 mm - 3.2 mm). The results also indicated a strong linear relationship between the abdominal motion and liver's SI motion and that higher order models (more complex models) did not improve the overall fit of the data. Furthermore, the results show that using only one marker would result in a lower accuracy than using multiple markers. Such conclusion was also assessed by [16] and concluded the same results. Moreover, the location of the marker affects the estimation accuracy such that the closer the marker was from the umbilicus the higher the estimation accuracy. The results also illustrated the accuracy of the estimated SI liver motion such that the MAE ranged between 1.9 mm and 0.8 mm for the three regression models. The results demonstrated consistent performances compared to previous research studies on the liver and external markers as a surrogate [16], [33], ultrasound as a surrogate [7] and accelerometers as a surrogate [24]. In the same context, Lasso outperformed MVR and Ridge in the overall estimation accuracy. However, the spacial resolution of the acquired MRI liver images prevented a more detailed evaluation of the three models.

VII. CONCLUSION

In this paper, we developed and evaluated an RME approach to estimate the liver SI motion due to respiration. External markers placed on the human's abdomen were tracked using a digital camera. Abdominal motion tracking was chosen as a surrogate data due to its MRI compatibility, patient's comfort, independence (could operate in and out of the MRI), high temporal and spacial resolution and high correlation with the liver motion. The motion data (liver) and the surrogate data (markers) were used to fit supervised learning regression models that were used to estimate the motion data based on the surrogate data. Three supervised learning regression models were selected and their performance and accuracy were evaluated. To validate the proposed approach, human subject experiments were conducted. Three healthy subjects participated in the experiments in a total of six sessions three minutes each. The MRI acquired liver data and the camera acquired marker data were first segmented, processed and split into training and testing segments. The three motion models were then trained and the optimal model parameters were selected. The designed models were further evaluated upon the test data. The results showed that the markers succeeded in estimating the liver motion with a good accuracy (below 2 mm).

As mentioned in this paper, RME consists of three main categories (motion data, surrogate data and fitting method). Each of these categories significantly affects the overall performance of the RME framework. In this study, a low field MRI system was used to acquire the motion data which resulted in a low temporal and spacial resolution that limited the overall evaluation of the proposed framework. The most crucial improvement to the proposed framework is to acquire the motion data by using a more powerful MRI system. Acquiring images at a higher temporal resolution would significantly affect the performance since more data samples could be acquired which would reduce the scanning session. Moreover, acquiring images at a higher spacial resolution allows investigating other liver motions (AP and lateral motions) that were not investigated due to the low spacial resolution and the relatively small motion in these directions. Obtaining higher spacial resolution of the motion data will result in a finer feature and shrinkage parameter tuning since the minimum values of these parameters are sharper. In the same context, the experiments were conducted at the University of Twente on healthy subjects with no lesions or fiducial internal markers present in the liver. Thus, estimating a specific region of interest in the liver was rather challenging. Moreover, anatomical features (such as the gall bladder or vessels) could have been chosen as the region of interest. However, tracking such anatomical features were challenging since their motion were inconsistent during the acquired sessions. As a result, further improvements could involve additional experiments on subjects or patients with implanted fiducial markers or lesions in the liver. Such fiducial or lesions could be positively identified and thus their 3D motion could be tracked.

In addition, temporal alignment was performed by acquiring the timestamps of the motion data and surrogate data independently since the MR system prevented any signal triggering from/to the system. Thereupon, using a common clock or signal triggering to both MRI and camera acquisition would improve the estimation accuracy as well as significantly preventing unnecessary post-processing errors. As illustrated in the results, the differences between the three regression models were not significant. Thus, using a

more complex regression algorithm would not improve the estimation accuracy significantly [35]. In fact, as explained before, shrinkage regression methods (such as Ridge and Lasso) outperform MVR in case of high dimensional data. Thus, using more than two markers will increase the system dimensionality and thus improve the estimation accuracy in Ridge and Lasso. In fact, multiple markers has been used in previous studies that indicated that using multiple markers will increase the system dimensionality that might capture more complex breathing patterns [16], [35]. Finally, using multiple surrogates could improve the overall performance by increasing the system dimensionality [31]. For example, [44] suggested that augmenting external markers with lung volume measurement (spirometers) might be used to improve the correlation accuracy.

To sum up, the objectives of this paper were to (1) choose appropriate surrogates and fitting algorithms that fit the MR environment alongside having a strong correspondence to the motion data and (2) validating such approach on human subjects. In deed, the objectives were met clearly such that it was justified earlier in this paper that abdominal tracking was the optimal surrogate choice. Accordingly, MVR, Ridge and Lasso were chosen and validated on human subjects throughout six sessions. The authors of this paper designed, implemented and validated an MRI acquired RME of liver with abdominal motion as a surrogate which was not addressed before in the literature. The authors also excelled by implementing Lasso regression which was also not addressed in the literature. Moreover, the authors surpassed other existing literature who utilized supervised learning in RME by explicitly implementing and analyzing the features and shrinkage parameters of the motion models. In fact, to the authors' knowledge, analyzing the features and shrinkage parameters of the learning models were not mentioned priorly in the existing literature in RME.

REFERENCES

[1] S. R. Abdel-Misih and M. Bloomston, "Liver anatomy," *Surgical Clinics of North America*, vol. 90, no. 4, pp. 643–653, 2010.

[2] "Cijfers over kanker, nederlandse kankerregistratie," accessed August 2017. [Online]. Available: http://www.cijfersoverkanker.nl/

[3] "World health organization, cancer key facts," Feb 2017, accessed August 2017. [Online]. Available: http://www.who.int/mediacentre/factsheets/fs297/en/

[4] R. A. Oberfield, G. Steele, J. L. Gollan, and D. Sherman, "Liver cancer," *CA: a cancer journal for clinicians*, vol. 39, no. 4, pp. 206–218, 1989.

[5] M. Abayazid, T. Kato, S. G. Silverman, and N. Hata, "Using needle orientation sensing as surrogate signal for respiratory motion estimation in percutaneous interventions," *International Journal of Computer Assisted Radiology and Surgery*, 2017.

[6] B. Stemkens, R. H. Tijssen, B. D. de Senneville, H. D. Heerkens, M. van Vulpen, J. J. Lagendijk, and C. A. van den Berg, "Optimizing 4-dimensional magnetic resonance imaging data sampling for respiratory motion analysis of pancreatic tumors," *International Journal of Radiation Oncology* Biology* Physics*, vol. 91, no. 3, pp. 571–578, 2015.

[7] F. Preiswerk, M. Toews, C.-C. Cheng, y. G. Chiou Jr, C.-S. Mei, L. F. Schaefer, W. S. Hoge, B. M. Schwartz, L. P. Panych, and B. Madore, "Hybrid mri-ultrasound acquisitions, and scannerless real-time imaging," *Magnetic resonance in medicine*, 2016.

[8] K. Langen and D. Jones, "Organ motion and its management," *International Journal of Radiation Oncology* Biology* Physics*, vol. 50, no. 1, pp. 265–278, 2001.

[9] P. J. Keall, G. S. Mageras, J. M. Balter, R. S. Emery, K. M. Forster, S. B. Jiang, J. M. Kapatoes, D. A. Low, M. J. Murphy, B. R. Murray *et al.*, "The management of respiratory motion in radiation oncology report of aapm task group 76," *Medical physics*, vol. 33, no. 10, pp. 3874–3900, 2006.

[10] J. Ehrhardt, C. Lorenz *et al.*, *4D Modeling and estimation of respiratory motion for radiation therapy*. Springer, 2013.

[11] S. Shimizu, H. Shirato, B. Xo, K. Kagei, T. Nishioka, S. Hashimoto, K. Tsuchiya, H. Aoyama, and K. Miyasaka, "Three-dimensional movement of a liver tumor detected by high-speed magnetic resonance imaging," *Radiotherapy and oncology*, vol. 50, no. 3, pp. 367–370, 1999.

[12] K. E. Barrett *et al.*, "Ganong's review of medical physiology," 2010.

[13] J. R. McClelland, D. J. Hawkes, T. Schaeffter, and A. P. King, "Respiratory motion models: a review," *Medical image analysis*, vol. 17, no. 1, pp. 19–42, 2013.

[14] H. Lal, Z. Neyaz, A. Nath, and S. Borah, "Ct-guided percutaneous biopsy of intrathoracic lesions," *Korean journal of radiology*, vol. 13, no. 2, pp. 210–226, 2012.

[15] Y. Zhou, K. Thiruvalluvan, L. Krzeminski, W. H. Moore, Z. Xu, and Z. Liang, "Ct-guided robotic needle biopsy of lung nodules with respiratory motion–experimental system and preliminary test," *The International Journal of Medical Robotics and Computer Assisted Surgery*, vol. 9, no. 3, pp. 317–330, 2013.

[16] F. Ernst, V. Martens, S. Schlichting, A. Beširević, M. Kleemann, C. Koch, D. Petersen, and A. Schweikard, "Correlating chest surface motion to motion of the liver using ε-svr–a porcine study," *Medical Image Computing and Computer-Assisted Intervention–MICCAI 2009*, pp. 356–364, 2009.

[17] A. S. Beddar, K. Kainz, T. M. Briere, Y. Tsunashima, T. Pan, K. Prado, R. Mohan, M. Gillin, and S. Krishnan, "Correlation between internal fiducial tumor motion and external marker motion for liver tumors imaged with 4d-ct," *International Journal of Radiation Oncology* Biology* Physics*, vol. 67, no. 2, pp. 630–638, 2007.

[18] F. Odille, N. Cîndea, D. Mandry, C. Pasquier, P.-A. Vuissoz, and J. Felblinger, "Generalized mri reconstruction including elastic physiological motion and coil sensitivity encoding," *Magnetic resonance in medicine*, vol. 59, no. 6, pp. 1401–1411, 2008.

[19] M. White, D. Hawkes, A. Melbourne, D. Collins, C. Coolens, M. Hawkins, M. Leach, and D. Atkinson, "Motion artifact correction in free-breathing abdominal mri using overlapping partial samples to recover image deformations," *Magnetic resonance in medicine*, vol. 62, no. 2, pp. 440–449, 2009.

[20] T.-N. Nguyen, J. Moseley, L. Dawson, D. Jaffray, and K. Brock, "Adapting liver motion models using a navigator channel technique," *Medical physics*, vol. 36, no. 4, pp. 1061–1073, 2009.

[21] J. Hinkle, P. T. Fletcher, B. Wang, B. Salter, and S. Joshi, "4d map image reconstruction incorporating organ motion," in *International Conference on Information Processing in Medical Imaging*. Springer, 2009, pp. 676–687.

[22] E.-J. Rijkhorst, I. Rivens, G. t. Haar, D. Hawkes, and D. Barratt, "Effects of respiratory liver motion on heating for gated and model-based motion-compensated high-intensity focused ultrasound ablation," in *Proceedings of the 14th international conference on Medical image computing and computer-assisted intervention-Volume Part I*. Springer-Verlag, 2011, pp. 605–612.

[23] C. Buerger, R. E. Clough, A. P. King, T. Schaeffter, and C. Prieto, "Nonrigid motion modeling of the liver from 3-d undersampled self-gated golden-radial phase encoded mri," *IEEE transactions on medical imaging*, vol. 31, no. 3, pp. 805–815, 2012.

[24] B. Chen, N. Weber, F. Odille, C. Large-Dessale, A. Delmas, L. Bonnemains, and J. Felblinger, "Design and validation of a novel mr-compatible sensor for respiratory motion modeling and correction," *IEEE Transactions on Biomedical Engineering*, vol. 64, no. 1, pp. 123–133, 2017.

[25] J. D. Hoisak, K. E. Sixel, R. Tirona, P. C. Cheung, and J.-P. Pignol, "Correlation of lung tumor motion with external surrogate indicators of respiration," *International Journal of Radiation Oncology* Biology* Physics*, vol. 60, no. 4, pp. 1298–1306, 2004.

[26] Q. Xu and R. J. Hamilton, "A novel respiratory detection method based on automated analysis of ultrasound diaphragm video," *Medical physics*, vol. 33, no. 4, pp. 916–921, 2006.

[27] D. A. Low, T. Zhao, B. White, D. Yang, S. Mutic, C. E. Noel, J. D. Bradley, P. J. Parikh, and W. Lu, "Application of the continuity equation to a breathing motion model," *Medical physics*, vol. 37, no. 3, pp. 1360–1364, 2010.

[28] D. Yang, W. Lu, D. A. Low, J. O. Deasy, A. J. Hope, and I. El Naqa, "4d-ct motion estimation using deformable image registration and 5d respiratory motion modeling," *Medical physics*, vol. 35, no. 10, pp. 4577–4590, 2008.

[29] C. Santelli, R. Nezafat, B. Goddu, W. J. Manning, J. Smink, S. Kozerke, and D. C. Peters, "Respiratory bellows revisited for motion compensation: preliminary experience for cardiovascular mr," *Magnetic resonance in medicine*, vol. 65, no. 4, pp. 1097–1102, 2011.

[30] M. Henningsson and R. M. Botnar, "Advanced respiratory motion compensation for coronary mr angiography," *Sensors*, vol. 13, no. 6, pp. 6882–6899, 2013.

[31] R. Dürichen, L. Davenport, R. Bruder, T. Wissel, A. Schweikard, and F. Ernst, "Evaluation of the potential of multi-modal sensors for respiratory motion prediction and correlation," in *Engineering in Medicine and Biology Society (EMBC), 2013 35th Annual International Conference of the IEEE*. IEEE, 2013, pp. 5678–5681.

[32] A. Schweikard, G. Glosser, M. Bodduluri, M. J. Murphy, and J. R. Adler, "Robotic motion compensation for respiratory movement during radiosurgery," *Computer Aided Surgery*, vol. 5, no. 4, pp. 263–277, 2000.

[33] S. Vedam, V. Kini, P. Keall, V. Ramakrishnan, H. Mostafavi, and R. Mohan, "Quantifying the predictability of diaphragm motion during respiration with a noninvasive external marker," *Medical physics*, vol. 30, no. 4, pp. 505–513, 2003.

[34] J. Wasza, P. Fischer, H. Leutheuser, T. Oefner, C. Bert, A. Maier, and J. Hornegger, "Real-time respiratory motion analysis using 4-d shape priors," *IEEE Transactions on Biomedical Engineering*, vol. 63, no. 3, pp. 485–495, 2016.

[35] M. Wilms, R. Werner, J. Ehrhardt, A. Schmidt-Richberg, H. Schlemmer, and H. Handels, "Multivariate regression approaches for surrogate-based diffeomorphic estimation of respiratory motion in radiation therapy," *Physics in medicine and biology*, vol. 59, no. 5, p. 1147, 2014.

[36] W. Lu, D. A. Low, P. J. Parikh, M. M. Nystrom, I. M. El Naqa, S. H. Wahab, M. Handoko, D. Fooshee, and J. D. Bradley, "Comparison of spirometry and abdominal height as four-dimensional computed tomography metrics in lung," *Medical physics*, vol. 32, no. 7, pp. 2351–2357, 2005.

[37] J. Friedman, T. Hastie, and R. Tibshirani, *The elements of statistical learning*. Springer series in statistics New York, 2001, vol. 1.

[38] T. Klinder, C. Lorenz, and J. Ostermann, "Free-breathing intra-and intersubject respiratory motion capturing, modeling, and prediction," *Proceedings of the Medical Imaging: Image Processing*, vol. 7259, p. 72590T, 2009.

[39] T. He, Z. Xue, W. Xie, and S. T. Wong, "Online 4-d ct estimation for patient-specific respiratory motion based on real-time breathing signals," in *International Conference on Medical Image Computing and Computer-Assisted Intervention*. Springer, 2010, pp. 392–399.

[40] T. Klinder, C. Lorenz, and J. Ostermann, "Prediction framework for statistical respiratory motion modeling," *Medical Image Computing and Computer-Assisted Intervention–MICCAI 2010*, pp. 327–334, 2010.

[41] G. James, D. Witten, T. Hastie, and R. Tibshirani, *An introduction to statistical learning*. Springer, 2013, vol. 112.

[42] A. E. Hoerl and R. W. Kennard, "Ridge regression: Biased estimation for nonorthogonal problems," *Technometrics*, vol. 12, no. 1, pp. 55–67, 1970.

[43] R. Tibshirani, "Regression shrinkage and selection via the lasso," *Journal of the Royal Statistical Society. Series B (Methodological)*, pp. 267–288, 1996.

[44] N. Koch, H. H. Liu, G. Starkschall, M. Jacobson, K. Forster, Z. Liao, R. Komaki, and C. W. Stevens, "Evaluation of internal lung motion for respiratory-gated radiotherapy using mri: Part i—correlating internal lung motion with skin fiducial motion," *International Journal of Radiation Oncology* Biology* Physics*, vol. 60, no. 5, pp. 1459–1472, 2004.

3 Conclusion, Limitations and Future Recommendations

3.1 Conclusion

In this context, we developed and evaluated a novel approach to estimate the respiratory induced motion of the liver by tracking abdominal markers placed on the human's abdomen. Abdominal motion tracking was chosen as a surrogate data due to its MRI compatibility, patient's comfort, independence (could operate in and out of the MRI), high temporal and spacial resolution and high correlation with the liver motion. With the MRI acquired liver motion as a motion data and abdominal tracking as a surrogate data, three supervised learning algorithms were designed and analyzed to fit both data. Accordingly, three motion models were developed to estimate the liver motion. The proposed approach was validated by conducting human subject experiments. Six sessions were performed on three subjects. Furthermore, the acquired data were processes offline and the models were designed. The results showed that developed approach sucessfully estimated the liver motion with a good accuracy (less than 2mm).

To summarize, the objectives of this paper were to (1) choose appropriate surrogates and fitting algorithms that fit the MR environment alongside (2) validating such approach on human subjects. In deed, the objectives were met clearly such that it was justified earlier in this paper that abdominal tracking was the optimal surrogate choice. Accordingly, three algorithms were chosen and validated on human subjects throughout six sessions.

3.2 Limitations and Future Recommendations

The limitations of this context are addressed as follows:

- A low field open bore MRI was used to conducted the motion data. The MRI system had limited spacial and temporal resolutions which limited the overall analysis and performance of the proposed approach. As a result, the limited spacial resolution restricted the analysis of the liver motion to the superior-inferior direction only.
- No internal fiducial markers or lesions were present during the experiments due to the fact that the experiments were conducted on healthy subjects. As a result, motion tracking was limited to the liver border rather than a certain motion of interest.
- Temporal synchronization was performed by acquiring the relative timestamps of the motion and surrogate data independently due to the fact that the MRI system prevented any input/output triggers or communication with other hardware and/or computers.

Accordingly, the following recommendations are suggested:

- Conducting the experiments on a more powerful MRI that is equipped with a relatively higher temporal and spacial resolution. Such improvement would result in a better estimation accuracy as well as more understanding to the fitting algorithms. Moreover, such an improvement will result in investigating the estimation accuracy of the liver in the other directions (inferior-posterior and lateral).
- Conducting the experiments on patients that bear implanted fiducial or hepatic lesions.
- Using a common clock or signal triggering to both MRI and and camera acquisition which would result in improving the estimation accuracy and preventing additional processing errors.

Appendix [A]: Measurement Protocol

A.1 Pre Scan Preparation

- Clean Scrub trousers should be ready for the subject.
- The clothes hanger (coat stand) available in the MRI room is used to place the laptop used for camera acquisition. The hanger is to be placed close to the MRI cage.
- Coil is placed on the MRI table
- Back, feet, elbow and head cushions are placed on the MRI table. The cushions positions will be further adjusted during subject positioning. The back cushion is to be placed with the thinner cross section is to the left of the MRI system as shown in figure 1.
- Tissue is placed above the back cushions.
- The MRI PC's clock should be checked and compared to the camera's laptop. The exact time difference (rounded to one second) is to be noted.
- The camera is to be mounted on the tripod and ready to be positioned according to the camera positioning in. The camera acquisition protocol should be ready and on stand by for further adjustments.
- Subject is requested to enter the MRI cage.

A.2 Initial Subject Preparation

- Subject is asked if there are any unclear questions.
- Screening and Eligibility checklist is to be signed. A copy of the checklist should be printed before hand in case the subject did not provide it. Subject will be informed that he/she might hear some noise during the 9-minute scan.
- Any metallic/Ferrous material is to be removed by the subjects and the investigators who will enter the MRI cage.
- Subject will put on the scrub trousers. Male subjects will remain topless and female subjects will put on a sport (non-metallic) bra.

A.3 Subject Positioning and MRI Acquisition

- Subject positioned in supine motion with head is to the left of the MRI system (as shown in figure 1).
- Coil #17 from Esaote is placed (internal height and width dimensions are 288 mm and 470 mm respectively).
- First level subject positioning:
  - Subject to be adjusted for initial placement such that the armpits are approximately touching the coil.
- Second level of subject positioning:
  - Using the localizer of the MRI system in transverse plane, the subject is positioned in the lateral direction until the spine is in the middle of the coronal plane.

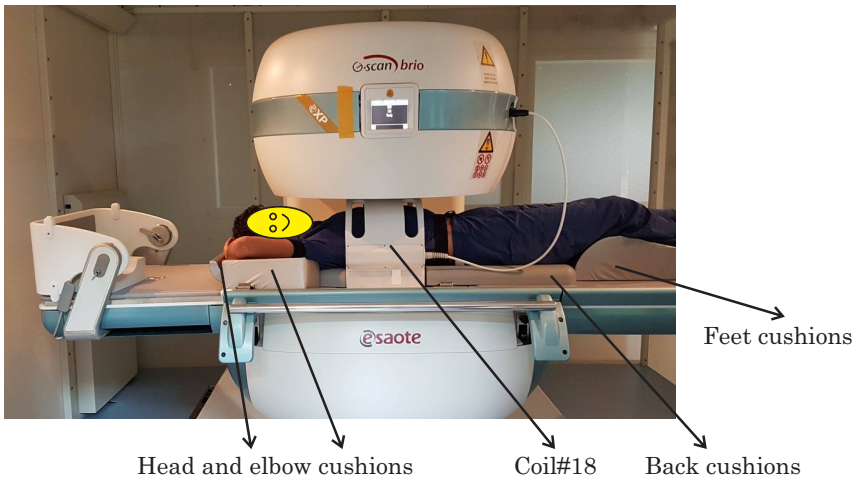

Figure 1: Subject Positioning

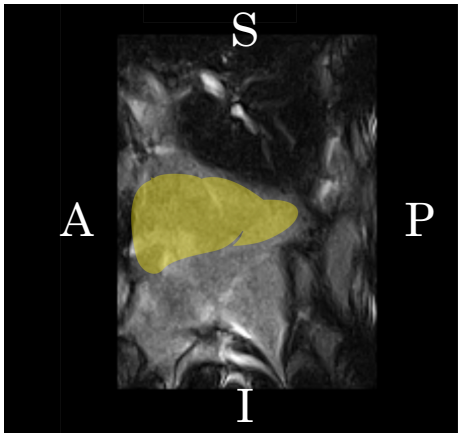

Figure 2: Expected MR Liver Image: Sagittal Plane

  - Using the localizer of the MRI system in coronal plane, the subject is positioned in the superior inferior direction until the liver and lung are observed. A brighter anatomy during exhalation indicates the liver while a darker anatomy during inhalation indicates the lung.

- Third level of subject positioning:

  - The investigators will perform a second localizer sequence on the MRI system's software in sagittal plane such that the liver is clearly seen in sagittal view and the liver is in the middle of the superior inferior view of the acquired image. At this step the images should be expected to be as shown in figure 2.

- A predefined sequence will be performed. The MRI sequence is a 0^{o} 2DHYCES, sagittal plane, slice thickness = 15 mm, repetition time = 7, echo time = 3.5, speedup = 150, encoding direction = H-F, acquired resolution = 1.8 mm x 1.8 mm, reconstructed resolution = 1.5 mm x 1.5 mm, flip angle = 40, field of view = 38x38, temporal resolution approximately 1 fps, and slice location is approximately 60-70 mm outside the coil center (first start with 60 mm, if the liver's upper boundary is not clearly visible, increase the location to 65 mm and if still not visible increase the location to 70 mm) and approximately 45 mm outside the spinal center.

AT THIS STEP MRI ACQUISITION IS ON STANDBY

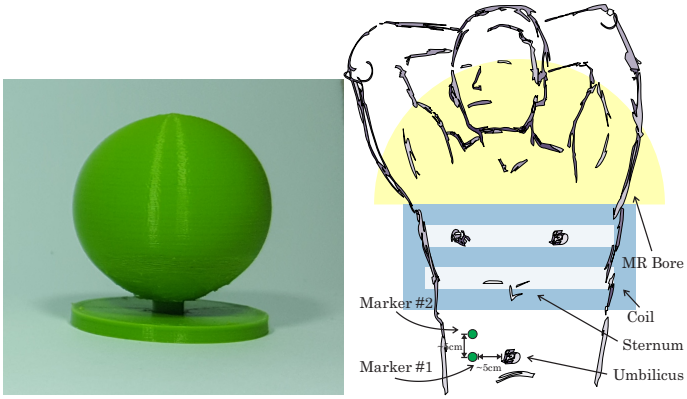

Figure 3: Marker Positioning

A.4 Marker Positioning

- 2 cm diameter markers are chosen during this study as shown in the left of figure 3. A double face sticker tape is used to stick the marker on the subject's body.
- As shown in the right of figure 3, two markers are going to be placed. Both markers are going to be placed approximately 5 cm to the right of the subject's umbilicus. The first marker is coinciding horizontally to the subject's umbilicus while the second marker is to be placed approximately 4-8 cm above the first marker. The second marker should also be approximately 4 cm from the used coil.

A.5 Camera Positioning and Acquisition

- The camera's depth (relative to the patientâĂŹs position) is placed at the MRI cage's door approximately 2 m deep from the center of the MR system as shown in figure 4.
- The camera's vertical position is approximately placed 1.48 m from the floor's ground. The camera's horizontal position is to be placed such that the tripod (fully extended) is touching the MRI cage's door (fully opened).
- The final orientation should be parallel to the subject's sagittal plane facing the markers.
- Predefined video acquisition parameters are chosen (brightness, gain, saturation, exposure, fps, special resolution, region of interest, etc.).

AT THIS STEP CAMERA ACQUISITION IS ON STANDBY

A.6 Final Steps

- Initial image is taken for calibration by using a large checkerboard with known dimensions
- Subject is requested to breath normally from the mouth and try not to move during the scan
- Camera acquisition start
- MRI acquisition start
- 9 minutes scan is performed

AT THIS STEP THE SCAN IS COMPLETE

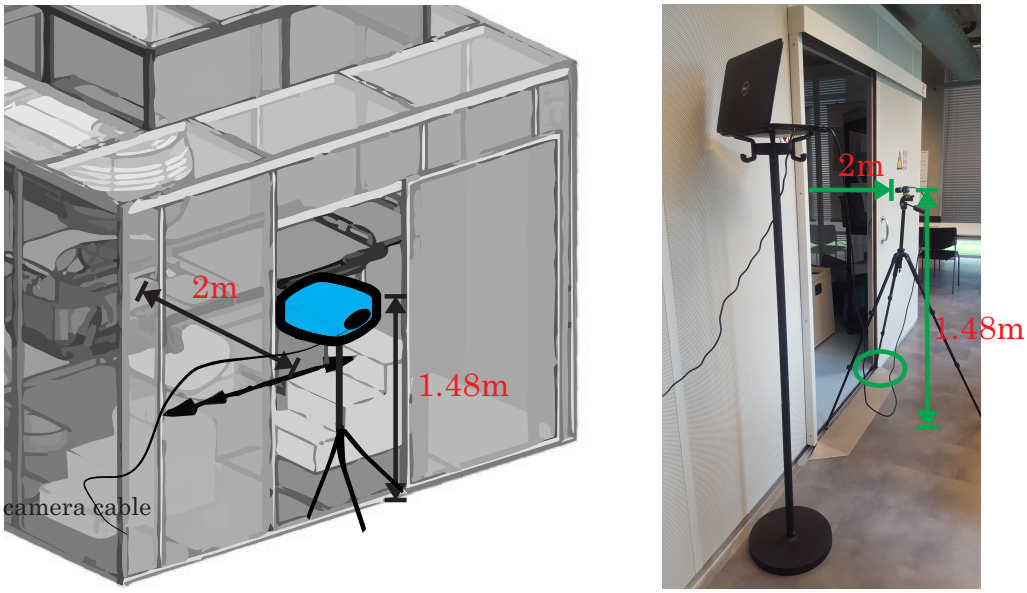

Figure 4: Camera Positioning

A.7 Post Scan

- MRI and Camera data are stored
- Camera is removed from the door
- Markers removed from Subject
- Subject leaves the MRI cage
- Subject changes his/her clothes and leaves the MR room

Appendix [B]: Subject Consent Form:

Respiratory Motion Estimation with Abdominal Motion as a Surrogate

Robotics and Mechatronics Lab, University of Twente *June, 2017*

Dear Sir or Madam,

You are asked to take part in a medical-scientific study. Participation is voluntary and it requires your written consent. You have received this letter because you are an eligible candidate for this study. Before you decide whether you want to participate in this study, you will be given an explanation about what the study involves. A member of our research team will also talk to you about taking part in this research study. Please read this information carefully and ask the investigator(s) for an explanation if you have any questions. All the contact details and the involved investigators are mentioned at the end of this document. You may also discuss it with your partner, friends or family.

Brief Background Information

Currently, imaging techniques are advancing widely in the medical field, such as in image-guided interventions and diagnosis. Among the available imaging techniques, magnetic resonance imaging (MRI) offers the highest soft tissue contrast, and this helps detecting small lesions (such as tumors) at an early stage. However, during percutaneous interventions (biopsy or ablation), MRI does not offer real-time image-guidance and thus the exact real time motion of the tumor is unknown. This will result in inaccurate targeting in case of percutaneous interventions and radio-therapy, and misdiagnosis in case of biopsy. In the same context, respiratory-induced motion is another major issue that results in inaccurate targeting and misdiagnosis. Several organs get affected by respiration especially the organs that are in the abdominal regions (lungs, diaphragm, liver, kidney, etc.).

For an accurate diagnosis and treatment, the exact motion of the organ of interest has to be known. One of the approaches used to compensate for respiratory motion is Respiratory Motion Estimation (RME) which depends on estimating the internal motion of the organ of interest by measuring external signals so called “surrogates”. Surrogate signals should have a strong correlation with the exact organ motion (motion data). Furthermore, a learning-based fitting algorithm is designed in order to estimate a mathematical motion model between the surrogates and the motion data. The choice of the surrogate data, the learning algorithm and the motion data depends crucially on the application that they are utilized in. RME is under huge development by many research labs, institutions and industries worldwide and the results obtained are promising.

Purpose of this study

As shown in figure 1, we are doing this research to determine if we can estimate the internal organ motion (motion data) due to respiration by measuring an external surrogate signal (surrogate data). In this study, the organ or motion is the liver and the surrogate signal is chosen to be the human’s chest motion. The human chest will be tracked by small sized markers and measured using an industrial camera. The motion of the liver will be measured by acquiring MR images. The two acquired data will be processed offline and a fitting algorithm will be designed to estimate a mathematical motion model such that based solely on tracking the external markers in real-time, the liver motion is estimated.

As a result, the aim of this study is to acquire MRI images of the liver motion due to respiration alongside with external markers placed on the human’s chest in order to first investigate the correlation between such data. The main focus is to investigate the feasibility of using such surrogate signals for estimating the liver motion and explore feasibility of the designed mathematical models.

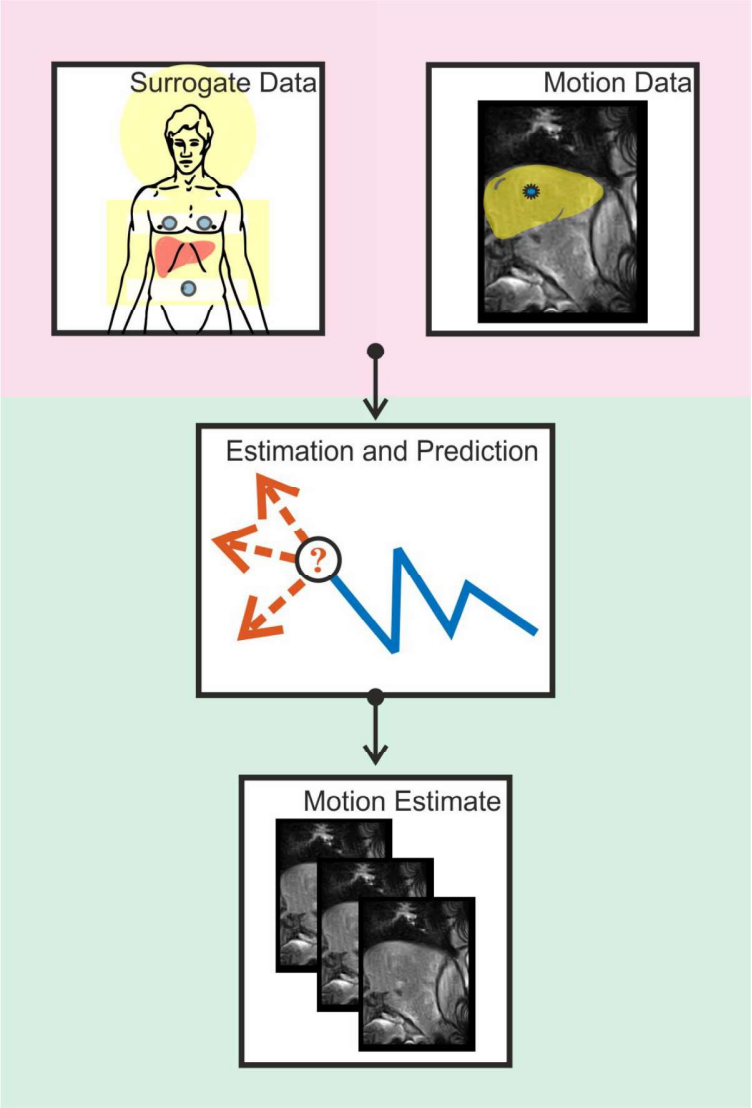

Figure1: System Overview

What is expected from you during this study?

a. Basic Procedures

The study will take place at the University of Twente using the G-Scan Brio MR system (0.25T) from ESAOTE as shown in figure 2. You will be subjected to a 9 minute scan in supine position. MR images will be acquired on your liver. Markers will be placed on your chest (as shown in figure 3) for camera tracking. The camera is placed outside the MR cage. The MR images and the chest motion will be recorded. These data will be processed offline to determine the relation between the respiratory phase, liver motion and chest motion. There will be no study visits except for the MRI scan itself. The total duration of the experiment will be approximately 60 minutes. After you agree to volunteer in the experiments and during the day of the experiment, the investigators will meet you to answer any unclear questions, make sure the MRI-use regulations are known by you, have the informed consent signed and prepare you for the scan. You will be then requested for a 9 minutes scan in the MRI room.

Figure2: G-scan Brio MR System from ESAOTE

Figure3: Subject Positioning

b. Scanning Procedures

The following points represent the steps and time-line of the study.

- First, the investigators will answer any unclear questions or concerns. You will then be present in the MRI room and the consent form (Appendix [A]), eligibility checklist and MR screening checklist (Appendix [B]) are checked by us and signed by you. You will be requested to remove any metallic materials (as informed by the consent form). In case you are a female, you will be requested to wear a sports bra without any ferrous material. Finally, you will be requested to enter the MRI cage.
- You will lay down on the MRI table in supine position with the hands behind the back. You will be placed such that the coil is until the subject's armpits as shown in figure 3. Your exact location from the coil will be further updated by localizing the liver from the MR system.
- After the correct placement, the markers will be placed on your chest then the camera will be adjusted outside the MRI cage.
- Consequently, the investigators will leave the MR cage and the camera will start recording. Simultaneously, 9 minutes of MR scan will be acquired and recorded.
- After the scan is completed. The recording will stop, the subject will be requested to leave the MR cage, and final check will be performed on you to make sure you leave the MR room safely.
- The total investment time required from you is 60 minutes consisting of 35 minutes pre-scanning, 9 minutes scanning and 15 minutes post-scanning.

Risks and Discomforts

The study is based on data recording of MRI liver scans. Additionally, a color marker will be attached to your chest. The camera will be away from the MRI bore and outside the MRI cage in order not to affect the scanning procedure. The scanning procedure itself will take 9 minutes.

The procedure should have no psychological risks. The G-scan Brio system is an open MRI system preventing claustrophobic feelings. This study introduces no radiation risks since MR imaging does not involve any ionizing radiation. The system is a low field MRI (0.25T) and the strength of the magnet is comparable to a magnet of a fridge. No contrast agents will be given to subjects. Furthermore, all your data will be kept confidential. Access to the database that includes the study identification number will be restricted to the principle investigator. Data will be identified by the study identification number alone. You can withdraw from the experiment anytime without giving reasons. Data gathered up till then will be used anonymously.

Unlikely Events

In case of an unlikely event related to the MRI usage or the marker, the experiment will be stopped immediately. In case the principle investigator notices an unexpected finding in the MRI images, the experiment will be stopped immediately and the findings will be handed to you for further assessment by your GP.

If I take part in this study, how will you protect my privacy?

We will collect data consisting of the camera images where the locations of the markers are recorded as well as general information regarding your gender and age. The camera will capture only the markers. Thus, neither your face nor your full body will be recorded. MR images will also be collected to measure the location of the liver. The recorded data will be stored by the study identification number and will be only accessible for the involved researchers. The study identification number will consist of the following identifier: “S#” where “S” stands for human subject and “#” is a number starting with “1” for the first subject and that increases by one for each successive subject. You will be identified solely by the “S#” designation. There will be separate files for all subjects enrolled in the study. These files will include the eligibility checklist and all collected data. Accurate and complete study records will be maintained. Finally, the study maybe published in a medical book or journal or used to teach others. However, your name or other identifying information will not be used.

What are the possible benefits from being in this research study?

There will be no direct benefit from your participation in this study. This study will assist in gathering data as a feasibility study for future developments. In future, gaining knowledge about liver and target motion due to respiration might allow researchers and doctors to do the following:

- Apply target motion compensation methods in order to achieve more accurate needle placement and consequently improved clinical outcomes of needle interventions in liver. This can reduce the amount of re-insertions and this can decrease the potential tissue damage and patient discomfort.
- Give a feedback to the doctor (during surgery and needle insertion) about whether the liver is within a safe margin of motion.
- In Other applications, for example, in radiotherapy (respiratory gated radiotherapy), the respiratory induced tumor motion is known and thus more accurate radiation targeting could be reached which results in applying less radiation on healthy tissues.

Any questions?

If you have any questions, please contact any of the principle investigators mentioned below.

Contact Details

Protocol Short Title	Liver Motion Estimation using External Markers
Coordinating Investigators	Dr. Ir. Momen Abayazid (M.Abayazid@utwente.nl) Robotics and Mechatronics Group Faculty of Electrical Engineering, Mathematics and Computer Science, University of Twente Dr. Ir. Frank Simonis (f.f.j.simonis@utwente.nl) M.Sc. Jordy van Zandwijk (j.k.vanzandwijk@utwente.nl) Magnetic Detection and Imaging Group Faculty of Science and Technology, University of Twente
Principle Investigator	B.Sc. Shamel Fahmi (a.m.s.b.m.fahmi@student.utwente.nl)

- I have read the subject information form. I was also able to ask questions. My questions have been answered to my satisfaction. I had enough time to decide whether to participate.
- I know that participation is voluntary. I know that I may decide at any time not to participate after all or to withdraw from the study. I do not need to give a reason for this.
- I know that some people can access my data. These people are listed in this information sheet.
- I consent to my data being used in the way and for the purpose stated in the information sheet.
- I want to participate in this study.

Name of study subject:

Signature: Date: __ / __ / __

I hereby declare that I have fully informed this study subject about this study. If information comes to light during the course of the study that could affect the study subject's consent, I will inform him/her of this in a timely fashion.

Name of investigator (or his/her representative):

Signature: Date:__ / __ / __

Appendix [B] Eligibility Check List

If you have any questions, please ask any of the investigators present.

General Eligibility Check

General Questions	Yes	No
Are you over the age of 18?		
Are you affiliated with the University of Twente?		
Do you have any known history of cancer or any terminal illness?		
Do you speak either Dutch or English?		
Do you have any contradictions with MRI?		

Subject: **S[ ]**

[Filled by investigator]

MR Screening Checklist

In the MRI-room, some implants, apparatus and objects can be damaged and/or cause damage to you. In order to exclude health risks as much as possible, anyone who is present in the MRI-room should carefully read and fill in the form.

MRI Use Questions	Yes	No
Do you have any metal (splinters) in your body, in particular in the eyes due to for example working in the metal industry (welding, working with lathes, etc.) or due to war violence (shackle, bullet residue, metal fragments)?		
Do you have a pacemaker, wires for a pacemaker or a defibrillator for your heart?		
Do you have a new heart/aorta valve or a stent?		
Do you have any clips in the vessels of the head or other vessels?		
Do you have any implanted magnets in your jaw?		
Do you have any hearing aids / bladder stimulator / insulin pump / neuro stimulator / baclofen pump / tissue expander?		
Do you have any ear or eye implants?		
Do you have any kidney deficiencies?		
Did you experience any allergic reaction to the contrast agent for MRI earlier?		
Are there any foreign materials present / implanted in your body?		
Are you pregnant?		
Only for MRI in the region of the head or neck: Do you have braces with metal that is secured in your mouth?		

Patch Medicine

Do you use any patch with a medicine called Rotigotine / Neupro? This patch contains aluminum and may not be in the MRI. You must remove the patch before the investigation. After the investigation, you can put on a new patch.

Pay Attention:

Metal, electrical or magnetically sensitive objects cannot enter the MRI cage because there is a strong magnetic field inside the cage. Think about credit cards, hearing aids, cell phone, watch, keys, hairpins, jewelry, glasses, bra (with metals inside) and coins.

Any more questions?

If not, please fill in this form and submit it to the person in charge.

Appendix [C]: Preliminary Experiments

C.1 Introduction

Before conducting the human subject experiments, multiple preliminary experiments were conducted and are presented in this appendix. The experiments included the following:

- MRI: Various sessions were conducted in the MRI room at the University of Twente to determine the optimal MRI sequence in addition to determining the subject positioning.
- Camera: Firstly, the camera was selected based upon defined specifications. Additionally, multiple sessions were conducted in and out of the MRI room to determine the optimal camera acquisition protocol and camera position.
- Marker Design and Locations: Three experiments were conducted (two outside and one inside the MRI room) to determine the optimal marker locations. The results of these experiments were mentioned in the paper. Prior to these experiments, the markers were designed and 3D printed.
- Fitting Algorithm (mock setup): A mock setup was designed by setting up a Lego© mechanism to mimic the breathing motion. The mock setup was used to test the overall framework before conducting any MRI Experiment.
- Dry Run: A final dry run experiment was conducted on one of the authors to test the entire human subject experiment before recruiting volunteers for the experiment.

During all the preliminary MRI sessions, only the principle investigators (authors of the paper) and the MRI investigators of the University of Twente participated. No subjects were included.

C.2 MRI Acquisition

Prior selecting the MRI sequence, the following specifications were required (from highest to lowest priority):

1. Temporal Resolution: As mentioned in the paper, the minimum temporal resolution to capture the respiratory induced motion was at 1 fps. Thus the MRI sequence should acquire MRI frames greater than or equal that update rate. Note that a higher update rate will result in a lower spacial resolution and image quality.
2. Spacial Resolution: The spacial resolution should be at least 10% of the superior-inferior motion of the liver. As stated by Langen et al., the average liver motion was 8.0 mm - 25.0 mm [7]. Thus, the spacial resolution of the acquired MRI frames should be 0.8 mm - 2.5 mm. Note that a higher spacial resolution will result in a lower temporal resolution.
3. Contrast and Signal-to-Noise ratio (SNR): The MRI sequence should acquire frames at high contrast and low SNR in order to efficiently detect the edge of the liver using image segmentation. Note that improving the image quality will reduce the temporal resolution.

In the same context, during these preliminary sessions, anatomical planes were also chosen. Since the superior-inferior motion in the liver is more dominant (one order of magnitude higher) than the other motions (anterior-posterior and lateral), either a sagittal or coronal were chosen. It was impossible at the required temporal and spacial resolution to acquire 3D motion at the MRI system. Thus, only one plane was selected (which was the sagittal plane). The final MRI sequence was mentioned in Appendix [A]. The chosen sequence was the most optimal

sequence according to the previous specifications. Fig. C.5 presents different frames acquired at during the MRI sequence selection procedures. The figure is arranged chronologically such that the final selected sequence is at the fourth row of the figure. Consequently, after selecting the MRI sequence, subject positioning (as Mentioned in Appendix [A]) was adjusted.

C.3 Camera Acquisition

In order to select an well-suited camera for the Respiratory Motion Estimation (RME) framework, the following specifications were required (from highest to lowest priority):

1. Temporal Resolution: The temporal resolution shall be greater than or equal to twice the breathing frequency. The update rate shall also be high enough to acquire and compute the estimated motion. Thus, the temporal resolution was selected as greater than or equal 10 fps.

2. Spacial Resolution: The spacial resolution should be chosen to be at least 10% of the smallest chest motion. During selecting the optimal marker locations, the mean chest motion was 3 mm - 10 mm in the anterior-posterior direction and 1.5 mm - 3 mm in the superior posterior direction. Thus, the spacial resolution was initially chosen to be 0.15 mm.

3. Region of Interest: The region of interest shall be wide enough (horizontally) to allow for tracking the markers (5 cm apart) with a 2 cm margin on each side to allow for the respiratory induced marker superior-inferior motion. Furthermore, the region of interest should be high enough (vertically) to allow for the respiratory induced marker anterior-posterior motion. As shown in Fig. C.6, the required field of view was initially chosen to be 300 mm × 200 mm (width × height) to allow for placing five markers.

4. Pixels: for a 300 mm × 200 mm region of interest of a 0.15 mm resolution, a camera of greater than or equal to 2.67 mega-pixel (MP) should be chosen.

As a result, the chosen camera was an mvBlueFox3-1031 color camera (H×V pixels = 2048×1536, sensor size = 1/2.3 inch, frame rate = 21 fps, USB3 interface, external input output (I/O)). Consequently, after camera selection, multiple sessions were conducted to optimize the camera location and acquisition. The camera was positioned out of the MRI cage while facing the subject's sagittal plane. Thus, the door of the MRI had to be open for the camera to track the markers. MRI scans were performed with the MRI door closed and opened and no observable difference in the quality of the images acquired from the MRI was noticed. As a result, the door was kept half-closed to give a narrow gap for the camera to track the markers. Camera acquisition was performed on a standard laptop equipped with an Intel(R) Core(TM) i5-4200 2.30 GHz and 8.00 GB RAM. During acquisition the laptop faced a significant challenge of memory usage such that the laptop used to shut down only after five minutes of acquisition (at the mentioned specifications above). As a result, in order to reduce the memory usage, a narrower region of interest was chosen to allow for tracking only two markers (thus the acquired region of interest was 200 mm wide × 150 mm high) which reduced the memory usage to the half.

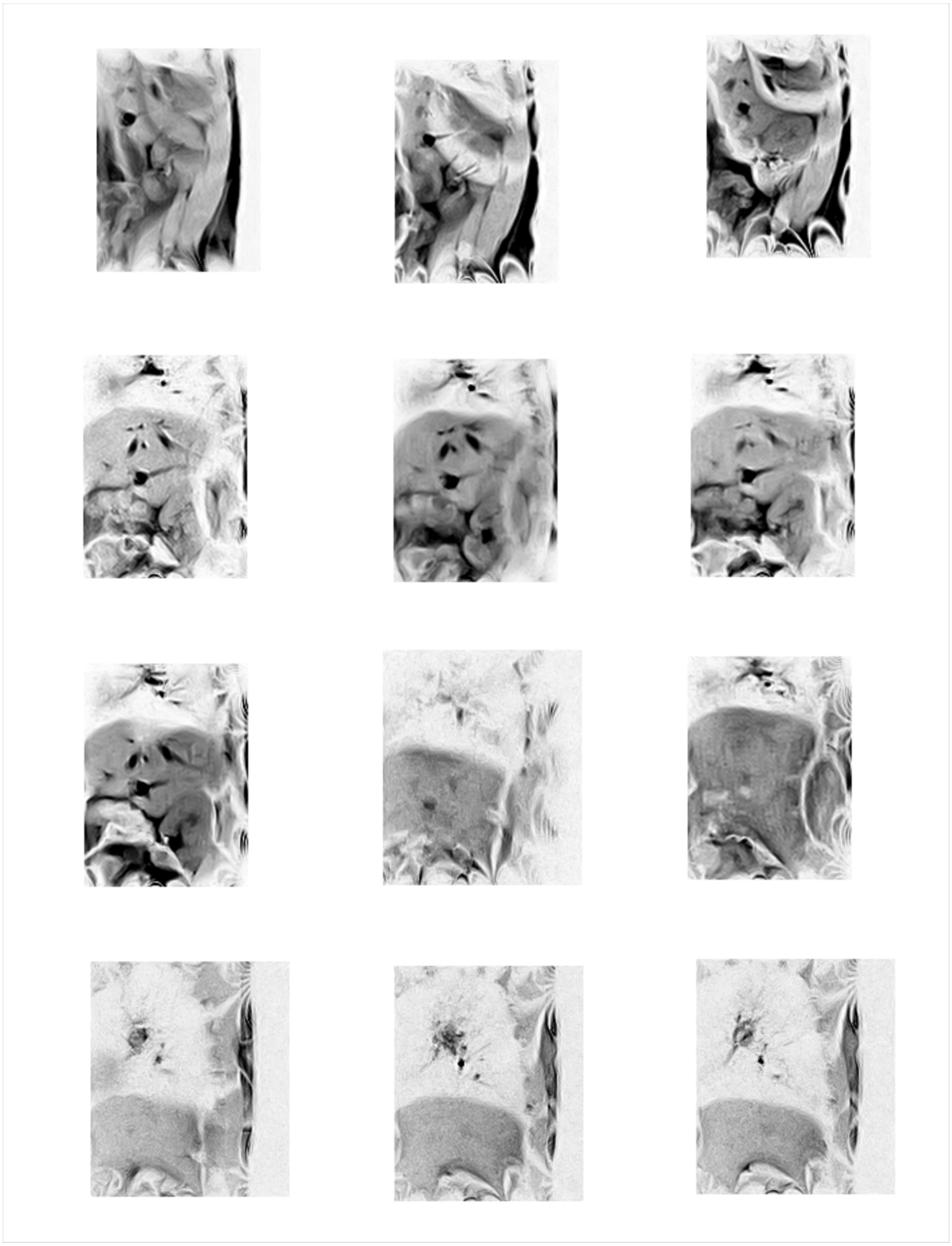

Figure C.5: MRI Acquisition: the figure illustrates the series of MRI sessions conducted to optimize the contrast and quality of the acquired liver frames. The figures are arranged chronologically such that the last row represents the chosen sequence. The figure is inverted for ink saving.

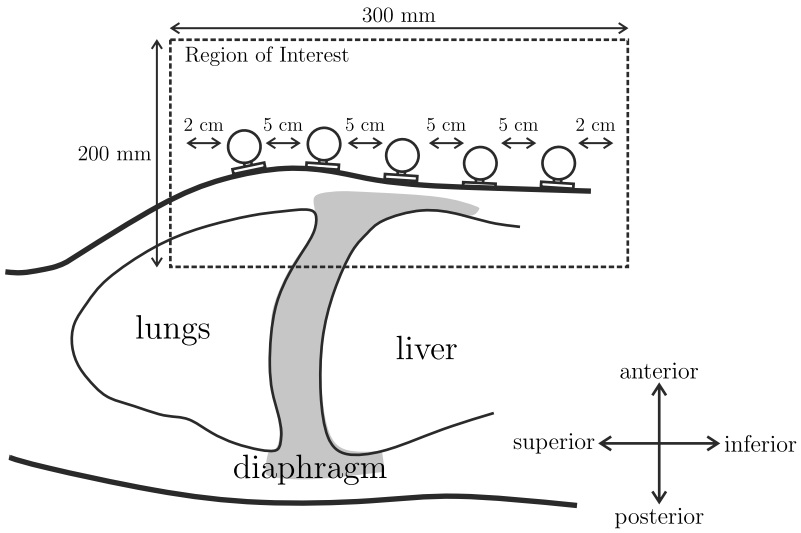

Figure C.6: Camera Acquisition: Region of Interest (ROI)

C.4 Mock Setup

To test the correspondence models prior the human subject's experiments, a mock up experiment was conducted by setting up a Lego© mechanism to mimic the breathing mechanics of the rib cage and the diaphragm. The mechanism was operated manually and tracked using a high definition (HD-1080p) web camera (Logitech C992 pro) at 30 fps. As shown in Fig. C.7, The right marker corresponds to the liver SI motion while the left marker corresponds to the chest AP and SI motions. The two markers were acquired for 150 seconds and the acquired data were split into 100 seconds for training and 50 seconds for testing. Likewise, the performance measure (MAE) was calculated to evaluate the estimation. As explained in the paper, the chosen correspondence models were MVR, Ridge and Lasso. The selected feature was a linear fit of one marker (Type 1 in the paper). The shrinkage parameters where 0.01 and 0.1 for Ridge and Lasso respectively.

The results of the mock setup are presented in Fig. C.8 and Table C.1. As shown in C.8, the three models managed to estimate the actual mimicked liver motion. There was no observed difference between the three models. However, as presented in Table C.1, MVR outperformed ridge and Lasso. Such results were expected since only one marker was used (thus no over-fitting to the data). Thus, shrinkage methods were not required in the presented setup. Note that the main outcome of this setup was to utilize such correspondence models and test them before the human subject experiments.

Table C.1: Evaluation Results: MAE and standard deviation $\boldsymbol{\sigma}$ of the estimated liver SI motion using MVR, Ridge and Lasso.

MVR	Ridge	Lasso
MAE	MAE	MAE
0.0378	0.0462	0.0401

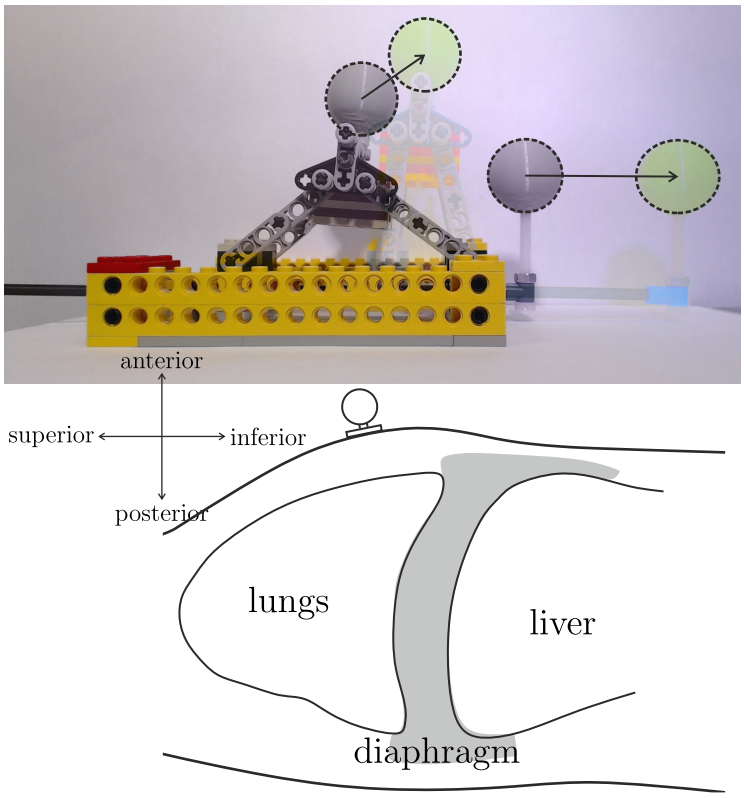

Figure C.7: Mock Setup: The figure illustrated the Lego mechanism of the mock setup. The set up mimics the motion of the liver and the ribcage due to respiration.

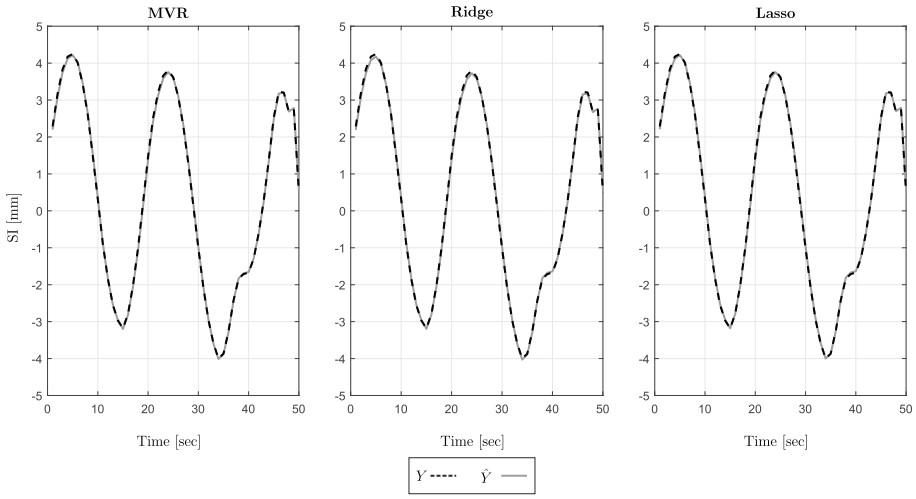

Figure C.8: Mock Setup: the figure represents the estimated value of the mimicked liver motion ($\hat{\boldsymbol{Y}}$) compared to the true values ($\boldsymbol{Y}$) for the three developed correspondence models. The MAE of the presented graphs are summarized in Table C.1.

Appendix [D]: Recruitment

The subjects were first recruited by handing out flyers (as shown in Fig. D.9) to students and employees from the University of Twente. After eligible candidates were selected, the consent form (Appendix [B]) was sent either as a hard copy to the volunteers or via email. The three volunteers agreed in participating and thus were invited to the MRI. The sessions were conducted during two consecutive days. The first subject came in the first day while the second and the third subject came the second day.

Figure D.9: Recruitment Flyer

Bibliography

(2017, accessed August 2017), World Health Organization, Cancer Key Facts. http://www.who.int/mediacentre/factsheets/fs297/en/

Ehrhardt, J., C. Lorenz et al. (2013), *4D Modeling and estimation of respiratory motion for radiation therapy*, Springer.

Keall, P. J., G. S. Mageras, J. M. Balter, R. S. Emery, K. M. Forster, S. B. Jiang, J. M. Kapatoes, D. A. Low, M. J. Murphy, B. R. Murray et al. (2006), The management of respiratory motion in radiation oncology report of AAPM Task Group 76, **vol. 33**, no.10, pp. 3874–3900.

Lal, H., Z. Neyaz, A. Nath and S. Borah (2012), CT-guided percutaneous biopsy of intrathoracic lesions, **vol. 13**, no.2, pp. 210–226.

Langen, K. and D. Jones (2001), Organ motion and its management, **vol. 50**, no.1, pp. 265–278.

McClelland, J. R., D. J. Hawkes, T. Schaeffter and A. P. King (2013), Respiratory motion models: a review, **vol. 17**, no.1, pp. 19–42.

Oberfield, R. A., G. Steele, J. L. Gollan and D. Sherman (1989), Liver cancer, **vol. 39**, no.4, pp. 206–218.

Preiswerk, F., M. Toews, C.-C. Cheng, y. G. Chiou Jr, C.-S. Mei, L. F. Schaefer, W. S. Hoge, B. M. Schwartz, L. P. Panych and B. Madore (2016), Hybrid MRI-Ultrasound acquisitions, and scannerless real-time imaging, *Magnetic resonance in medicine*.

Shimizu, S., H. Shirato, B. Xo, K. Kagei, T. Nishioka, S. Hashimoto, K. Tsuchiya, H. Aoyama and K. Miyasaka (1999), Three-dimensional movement of a liver tumor detected by high-speed magnetic resonance imaging, **vol. 50**, no.3, pp. 367–370.

Stemkens, B., R. H. Tijssen, B. D. de Senneville, H. D. Heerkens, M. van Vulpen, J. J. Lagendijk and C. A. van den Berg (2015), Optimizing 4-dimensional magnetic resonance imaging data sampling for respiratory motion analysis of pancreatic tumors, **vol. 91**, no.3, pp. 571–578.

Zhou, Y., K. Thiruvalluvan, L. Krzeminski, W. H. Moore, Z. Xu and Z. Liang (2013), CT-guided robotic needle biopsy of lung nodules with respiratory motion–experimental system and preliminary test, **vol. 9**, no.3, pp. 317–330.